Water-based lubricant containing protic ionic liquids and talc lubricant particles: Wear and corrosion analysis

Victor Velho de Castro [a,*], Leonardo Moreira dos Santos [b], Leonardo Marasca Antonini [a], Roberto Moreira Schroeder [a], Silvana Mattedi [c], Klester S. Souza [d], Marcelo Barbalho Pereira [e], Sandra Einloft [b], Carlos Alexandre dos Santos [b], Célia de Fraga Malfatti [a]

[a] *Department of Metallurgy, Laboratório de Pesquisa em Corrosão (LAPEC), Universidade Federal do Rio Grande Do Sul (UFRGS), Porto Alegre, Rio Grande do Sul, Brazil*
[b] *School of Technology, Pontifícia Universidade Católica do Rio Grande Do Sul (PUCRS), Porto Alegre, Rio Grande do Sul, Brazil*
[c] *Department of Chemical Engineering, Laboratório de Termodinâmica Aplicada, Universidade Federal da Bahia (UFBA), Salvador, Bahia, Brazil*
[d] *Department of Inorganic Chemistry, Laboratório de Bioanalítica, Universidade Federal Do Rio Grande do Sul (UFRGS), Porto Alegre, Rio Grande do Sul, Brazil*
[e] *Institute of Physics, Centro de Microscopia Óptica de Materiais – Grupo Laser & Óptica, Universidade Federal do Rio Grande Do Sul (UFRGS), Porto Alegre, Rio Grande do Sul, Brazil*

ARTICLE INFO

ABSTRACT

Water-based lubricants have been used in different industrial applications in recent years. However, studies evaluating the tribological and electrochemical effects of lubricants with Protic Ionic Liquid (PIL) and talc particles (TC) as additives on SAE 1010 and SAE 1045 steels are still scarce in the literature, which is the objective of this work. Samples extracted from steel sheets were investigated in the normalized (SAE 1010) and quenched-tempered (SAE 1045) conditions. Wear tests in a ball-on-plate type tribometer and corrosion tests using potentiondynamic polarization curves were performed in the presence of different lubricant solutions (PIL 3% + DI water, commercial lubricant 3% + DI water, with and without talc particle additions 0.05 and 0.1 wt%). Analyses of viscosity, pH, wettability, and particle size distribution were conduted on the lubricant and talc samples. Wear and corrosion surfaces were analyzed by SEM/EDS, and Raman techniques. The results showed that the tribofilm formed from the interaction between PIL lubricants and steel substrates decreased the wear due to the increase of lubricity of these lubricants. When the PIL and the commercial lubricants are compared, PIL additives presented higher performance, despite the talc addition. The influence of talc on the corrosion of steel is associated with the differential aeration effect, mitigated by adding the PIL.

1. Introduction

Water-based lubricants are used in numerous industrial applications such as metal forming, machining, oil extraction and assembly processes, as lubricant, cutting or hydraulic fluid, however, they often exhibit poor performance compared to petroleum-based lubricants [1]. Despite the low-cost and high-cooling capacity of the water, its low viscosity and corrosive properties make it inappropriate as a lubricant in tribological applications [2]. Therefore, an alternative to improve work performance of water-based lubricants is using high quality additives as active surface/interface molecules [3]. In general, these additives are solid nanoparticles, ionic liquids, and biobased oils. Aspects related to tribological properties and corrosion responses, as friction reduction and

oxidation resistance, respectively, are improved with these additives [1, 4] The main characteristics of lubricant additives that influence lubricity are ideal concentration, particle size and shape, and the secondary aspects are the microstructure and surface conditions of the substrate. Spherical particles, which have the potential to apply a very high surface tension, should be avoided in dispersions [5].

Ionic liquids (ILs) are liquid organic salts, composed of an anion, a cation, and at least one proton, which can form hydrogen bonds, which characterize these ionic liquids. ILs have shown immense potential for numerous applications, including energy storage devices, catalysis, biomass processing, pharmaceuticals, extractions, CO_2 capture [6]. Since the beginning of the 21st century, the use of ILs, as lubricants, has been studied [7–10]. Protic ionic liquids (PILs) have promising

---

molecules for use in lubrication, as they have properties required for a lubricant, such as high viscosity and low volatility, they are good solvents and potential uses as additives to reducing friction in various contacts [11,12]. Numerous works are using ionic liquids as additives, sometimes associated with solid phases (particles), as reported in the work of Avilés et al. [13], where the authors analyzed the tribological behavior of halogen-free PIL ionic liquids. The results showed that the coefficient of friction (COF) decreased throughout the test due to the evaporation of water from the emulsion. Other works analyzed the behavior of ILs as an additive in lubricants containing water [14]. In tribological tests with water-based lubricants, water evaporates after a certain testing period. When this occurs, there is a transition from a lubricated regime to a wearing regime without lubrication, leading to a consequent increase in the coefficient of friction (COF). However, in studies using PILs as additives, the formation of tribofilm was evidenced, which maintains lubrication even after water evaporation [13]. Tang and Li [15] presented a review of different promising products as future lubricants, confirming the great potential of ILs as lubricant due to adsorption, which occurs on the surface of the lubricated metal, with the consequent formation of tribofilm and reduced friction. Similar behavior was reported by Xiao et al. [25] considering the film thickness. Furthermore, they mentioned the potential that particles such as graphite, boron nitride, mica and poly(tetrafluoroethylene) (PTFE) have as lubricants in dispersions. The roughness of the shear surfaces can act as physical barriers that keep particles within the contact zones. This promotes an expected lubricating effect which consequently decreases wear [5].

In order to optimize the lubricity of water-based lubricants, many manufacturers have added lubricants with graphite particles [16–18], which have a high lubricating capacity. However, these particles cause galvanic corrosion when in contact with steel in aqueous solutions, further increasing the rate of steel corrosion. This is attributed to the very noble electrochemical potential of the graphite, which provides excellent sites for the development and acceleration of cathodic reactions. This corrosion increases at the same rate as the anode currents applied, because of the effects of galvanic couple formation between the graphite of the lubricant (which has nobler potentials) and steel (which has more active potential).

On the other hand, the use of solid lubricants has been known for centuries, as is the case of talc, for example, it can be used in lubricant formulations with applications in total loss of lubrication systems such as two-stroke engines and fuel systems, environmental awareness in agriculture and hydropower [19]. However, talc is rarely used as part of a lubricant composition based on water and PILs, and studies of water-based lubricants and PIL which analyze the tribological and electrochemical behavior of additives with talc particles are even rarer.

The aim of this study was to analyze the effect of the addition of talc particles in water-based lubricants with additives of a chosen PIL (that has lubricating properties [20], corrosion inhibiting capacity [21] and low toxicity [22] on the tribological and electrochemical responses of a low (SAE 1010) and a medium (SAE 1045) carbon steels. Lubricating capacities were tested in a ball-on-plate type tribometer, and lubrication and wear mechanisms determined through wettability, MEV/EDS and RAMAN analyses. Corrosion-inhibiting capabilities were determined through the electrochemical testing of potentiodynamic polarization curves. The performance of lubricants containing PIL was compared with that of lubricants with formulations containing a commercial additive.

2. Materials and methods

2.1. Characterization

In this work, six formulations involving deionized water, talc, PIL and a commercial additive were investigated as lubricants. Each component of the formulation, with exception of the DI water, is referred to by the term "additive". The water-based lubricants were obtained through the solubilization of protic ionic liquid (PIL) m-2HEAOL (Table 1), used as an additive in deionized water at a concentration of 3% (wt.%), hereafter referred to *m-2HEAOL_WP*. To compare performance, tests were also carried out with a commercial water-soluble lubricant, as an additive, in the same proportion of 3% (wt.%), identified as *Commercial_WP*. The lubricants were kept under mechanical agitation for 5 h, followed by a rest period for 24 h. *(WP means "without talc particles")*.

Schumacher brand talc particles, at concentrations of 0.05% (wt.%) and 0.1% (wt.%), were used as additives in PIL + H_2O and commercial additive + H_2O, labeled as *m-2HEAOL_TC_0.05%; m-2HEAOL_TC_0.1%; Commercial_TC_0.05% and Commercial_TC_0.1%*, respectively, as shown in Table 3. These concentrations are similar to those used by other authors [19]. After adding the particles, the lubricants were left to rest for 24 h. Before wear and corrosion tests, the dispersions were mechanically stirred for 30 min.

Brookfield viscosity was measured by a Brookfield Viscometer, model RVDV-I Prime (spindle SC4-21, 50 rpm and 100 rpm) at a temperature of 23 °C. The pH was determined with a Digimed pH meter, model Dm-22.

The particle size distribution (PSD) of talc particles was determined using a particle size analyzer, Cilas laser diffractometer, model 1180. The measurement was carried out in an aqueous medium, after 15 min on ultrasound. For X-ray diffraction (XRD) analysis, the talc particles were placed in the sample holder of a Shimadzu X-ray diffractometer, model XRD 7000. Cur Kα1 radiation was used for analysis, operating at 40 kV and 20 mA, 2θ angles ranged from 2° to 60° and step size 1°/s.

Samples of SAE 1010 steel, normalized at 800 °C, and SAE 1045 steel, austenitized at 850 °C, quenched in oil at 25 °C and tempered at 300 °C, were used in the study. These materials were chosen because they are used in numerous metalworking applications, such as rolling, stamping, forging, cutting, where lubricated conditions are usually required. The samples were grounded with silicon carbide sandpaper (#100, #220, #320, #400, #600, #1200), and later polished with 0.1 μm alumina solution. The chemical composition of the steels was analyzed in a Bruker spark emission spectrometer (OES), model Q2 ION. The microhardness was measured in a Mitutoyo microhardness tester, model HV-100, with a load of 50 g. Microstructures were analyzed in a Zeiss optical microscope, model Axio Lab. A1, after etching with Nital 3%. For image analyses, ZEN 2.6 software (blue edition) was used.

Average surface roughnesses (Ra and Rz) were measured in a Mitutoyo linear roughness meter, model SJ-400. Before the analyses, the samples were cleaned with water and neutral detergent, followed by ultrasound cleaning using acetone, after ethyl alcohol, and deionized water, for 15 min each, and finally dried using a hand-held hot air device.

2.2. Tribological test

A computationally controlled CETR Universal Micro Tribometer, model UMT-3, ball-on-plate configuration, was used in linear and reciprocal motion to evaluate the lubrication performance. The coefficient of friction (COF) was analyzed during the entire 1 h test (36 m sliding distance) with the samples immersed in the lubricants. The wear was performed by a 5 mm diameter Yttria Stabilized Zirconia sphere, Macea, grade 10, 1510 HV hardness, Ra = 0.020 μm roughness, according to the manufacturer. A normal force of 1 N and stroke of 5 mm was applied. The initial maximum and average hertzian contact pressure in the steel samples considering the elastic modulus (210 GPa) and Poisson's coefficient (0.33) were approximately 0.7 GPa and 0.63 GPa respectively, for SAE 1010 and SAE 1045 steels, and are within the surface tension range that most authors use in studies involving boundary lubrication [23]. In addition, very high surface tensions could make it impossible to study possible tribofilms formed [24]. In tests involving ball-on-flat reciprocating tribometer, frequencies lower than

Table 1
PIL used as additive in the investigated lubricants. Adapted from Vega et al. [28].

PIL	Structure
<u>m-2HEAOl</u> N-methyl – 2 – hydroxyethylammonium oleate	

8 Hz are not influenced by microstructural differences in the steels [25]. Thus, the frequency of 2 Hz was applied to evaluate the performance of the lubricant on both substrates. The external temperature was maintained at 21 °C and the lubricant temperature was monitored by a thermographic camera. The tests were carried out in triplicate for each condition. After the wear tests, the worn profiles were obtained using the Ambios contact profilometer, model XP-2. Three measurements of the cross-sectional area of three different points of the wear tracks were conducted. The average worn volume (V_m) of each system studied was calculated using Eq. (1), as recommended by the ASTM G133 standard method [26]:

$$V_m = A_m . CT \tag{1}$$

where: Am is the average area of the cross section of the track (mm^2).

CT is the total length of the stroke (mm).

Analyses of variance (ANOVA) of the results of the worn volumes were performed aiming to detect the statistical significance and possible synergistic effects between the studied input parameters [27–29]. The confidence level determined was 95% ($\alpha = 0.05$).

The specific wear rates (k coefficient) were calculated by Eq. (2) [30]:

$$k = \frac{V_m}{F . s} \tag{2}$$

where: *F* is the normal load (N).

s is the total sliding distance (m).

Considering that wear occurs on both flat specimen and ball (sphere), the worn volume of the counter body (ball) was determined by measuring the scar formed using the ZEN software (blue edition). The images of the spheres were obtained in the Zeiss Axio Lab. A1 optical microscope. The worn volume of the counterbody was calculated using Eqs. (3) and (4) [26]:

$$Vc = (\pi h / 6) \left[3D^2 / 4 + h^2 \right] \tag{3}$$

$$h = R - \left[R^2 - \left(D^2 / 4 \right) \right]^{1/2} \tag{4}$$

where: *D* is the mean scar diameter (mm).

R is the original radius of the sphere (mm);
h is height of material removed (mm).

The measurement error (*u()*) of the worn volume of the spheres was determined through equation (5) [31]:

$$u() \cong \frac{\pi a^3}{4R^2} \sqrt{\left(a^2 u(R)^2 + 16R^2 u(a)^2 \right)} \tag{5}$$

Where: *a* is the radius of the sphere wear scar.

u (R) is the measurement uncertainty of the sphere's radius (0.125 mm informed by the manufacturer).

u (a) is the measurement uncertainty of the scar radius of the sphere (measurement equipment sensitivity: 0.01 μm).

The wear mechanisms and the morphology of the talc particles were evaluated using a high-resolution scanning electron microscope, FEG-SEM Inspec, model F50. The wear tracks were also analyzed by Raman spectroscopy in a Horibam LabRamHr Evolution Laser Raman Spectrometer, model DXR (laser excitation wavelength of 532 nm), and Access alpha 300 (632.8 nm - micro-Raman single-spot analysis and mapping microscope).

To confirm the surface changes that occurred in the steel samples in contact with the lubricants, immersions were carried out for 1 h in the samples of both substrates. After immersions, wetting tests were carried out. Contact angle measurements were performed using the sessile drop method and apparatus developed by the Corrosion Research Laboratory (LAPEC) of the Federal University of Rio Grande do Sul (Porto Alegre, Brazil). The deionized water drop was observed through a low-magnification lens and the contact angle measured in Surftens 4.5 software.

2.3. Electrochemical tests

The inhibition capacity of the studied lubricants was determined through potentiodynamic polarization curves (PPC). Tests were carried out on lubricants containing the proposed maximum particle content (0.1% (%wt)) of talc. For comparison purposes, tests were also carried out containing deionized water and particles, in the concentration mentioned above. Thus, it was possible to compare the corrosion inhibition capacity of PIL and the commercial lubricant, as well as to evaluate the electrochemical effect of talc particles added to the lubricants. Assays were performed on both substrates mentioned above. CPP were obtained in an Autolab potentiostat from Metrohm, model PGSTAT302 N.

The three-electrode electrochemical cell consisted of the steel sample as a working electrode, against a platinum electrode and saturated calomel reference electrode. The reference electrode was immersed in a saturated KCl solution. Electrical contact was carried out through the salt bridge of a saturated KCl solution and agar-agar. Before the experiments, the working electrode was immersed in the test solution for 30 min and a less than 5 mV/s variation at the open circuit potential (OCP) was reached.

The potentiodynamic polarization curves were obtained from the E_{OCP} in the cathodic direction down to −800 mV below the E_{OCP}; then, samples were exchanged and immersed again for 30 min to stabilize the OCP. From the stabilization of the E_{OCP}, scanning was performed in the anodic direction, up to +1000 mV above the E_{OCP}. The scan rate used was 1.0 mV/s. The tests were carried out in triplicate for each condition. After CPP, surfaces of the samples were analyzed in a Zeiss Axio Lab. A1 optical microscope. Corrosion potentials (E_{Corr}) and corrosion current density (I_{Corr}) were obtained through Tafel extrapolation by electrochemical software NOVA version 2.1.4. And the corrosion rates were calculated according to ASTM G102 [32].

3. Results and discussion

3.1. Characterization of steel samples and lubricants

The chemical compositions of the steels are shown in Table 2, as well as the hardness and surface roughness of the samples. As observed, the amounts of main solutes are close to the specified values. The hardness values of the normalized SAE 1010 steel were about 127 ± 22.5 HV ($\cong$ 70 HRB) while the quenched-tempered SAE 1045 steel exhibited values of 540 ± 26 HV ($\cong$ 52 HRC). In both conditions, the average surface roughnesses were similar, and are in accordance with the ASTM G133 standard method (<0.03 μm). Fig. 1 shows the microstructures resulting from the different heat treatments used in the samples of normalized SAE 1010 and quenched-tempered SAE 1045 steels. In Fig. 1A, the predominance of an α-ferritic matrix is noted, with small lamellae pearlite islands located preferentially at the grain boundaries. The microstructure is characteristic of low carbon steel alloys cooled under low cooling conditions. The heat treatment of quenching (850 °C) followed by tempering (300 °C) resulted in a tempered martensitic microstructure in the SAE 1045 steel samples (Fig. 1B), with hardness values superior to that of the samples of SAE 1010 steel.

The lubricants investigated in this work are shown in Table 3. A difference of approximately 10 mPa s can be seen in the viscosity values obtained at 100 RPM when comparing IL with commercial lubricants, while at 100 RPM the values were the same. Therefore, the lubricants containing m-2HEAOL are slightly more viscous than the lubricants containing commercial additives. It is known that lubricants with higher viscosities tend to show better lubricity in hydrodynamic lubrication regimes and, consequently, influencing the minimum thickness in the lubricant film that separates two surfaces in relative motion [33]. Furthermore, significant changes in lubricants containing talc particles in the proportions of 0.05% (wt) and 0.1% % (wt) were undetected in the viscosity tests.

The pH values of the lubricants were similar, with PIL lubricants being slightly more alkaline, especially when compared to the commercial lubricant combined with talc particles. A more alkaline pH of lubricants containing m-2HEAOL may be associated with the presence of free electrons in the amino group in the structure of LI ($-NH_2$) and of the hydroxyl group (-OH). Furthermore, the presence of polarity in the molecule and its ionic characteristic also contribute to a higher pH. Possibly, the differences observed in pH values and viscosity measurements between the commercial additive and PIL m-2HEAOL, may be associated with differences in their molecular structure.

Fig. 2A shows the particle size distribution (PSD) of the talc microparticles. The distribution of equivalent diameters is close to a Gaussian distribution. As for the particle size, 90% of the particles have dimensions up to 59.8 μm, 50% of the particles are up to 23.7 μm and 10% are up to 6.8 μm. The average particle diameter was approximately 29.6 μm. Previous works showed that particles with dimensions greater than 0.5 μm are not the most suitable for lubricating conditions, as they do not produce a stable suspension due to the precipitation tendency of the suspended particles. Consequently, it is more difficult to fill in peaks and valleys on the surface due to their large dimensions [15,34]. However, in addition to the known lubricating capacity of talc resulting from its structure [35], the lamellar shape seen in talc particles (Fig. 2B) can contribute to increased lubricity. According to Akbulut [5], particles with a similar shape to bars can be deposited between the peaks of the surfaces in contact and in relative movement, contributing to increase in lubricity and decrease in wear. From the XRD analysis (Fig. 2C), it was

Table 3
Composition, viscosity, and pH of the studied lubricants.

Lubrificant	Composition (wt. %)	Viscosity 50 RPM (mPa.s)	Viscosity 100 RPM (mPa.s)	pH
m-2HEAOL_WP	H_2O + 3% m-2HEAOL	20 (±0.5)	30 (±0.5)	8.0 (±0.5)
m-2HEAOL_ TC _0.1%	H_2O + 3% m-2HEAOL + 0.1% Talc	20 (±0.5)	30 (±0.5)	8.3 (±0.5)
m-2HEAOL_ TC _0.05%	H_2O + 3% m-2HEAOL + 0.05% Talc	20 (±0.5)	30 (±0.5)	8.8 (±0.5)
Commercial_WP	H_2O + 3% commercial additive	20 (0.5)	20 (0.5)	8.4 (0.5)
Commercial_TC_0.05%	H_2O + 3% commercial additive + 0,05% Talc	20 (0.5)	20 (0.5)	7.8 (0.5)
Commercial_TC_0.1%	H_2O + 3% commercial additive + 0.1% Talc	20 (0.5)	20 (0.5)	7.2 (0.5)

possible to detect only magnesium silicate hydroxide phases, talc (JCPDS NO. 01-073-0147) and vermiculite (01-074-1732), with no detectable presence of contaminants.

Fig. 3 shows the results of contact angle after immersion in the studied lubricants. Due to the low corrosion resistance of the steel samples, it was not possible to immerse the samples for 1 h in H_2O and H_2O with 0.1% (%wt.) TC. These samples were immersed for 2 min. The immersion in H_2O practically unchanged the contact angle of deionized water with the surface of both substrates, with values in the range of 30°–33° and 40°–43° for SAE 1010 and SAE 1045 steels, respectively. However, immersion in the formulation containing H_2O and 0.1% talc increased the contact angle values, leaving the surfaces more hydrophobic. Adhesive interactions between talc and water are strong enough to overcome unfavorable entropy, so water is adsorbed onto the talc surfaces in environments with low relative humidity. However, these interactions are weak to surpass the cohesive interactions of water. Thus, the presence of a second water molecule weakens the water-surface interactions, which need to compete with the cohesive interactions between the water molecules [36]. Therefore, in environments with high humidity, it is easier for water molecules to escape from the talc surface, generating hydrophobic behavior [36]. Talc particles have two faces: the hydrophobic basal surface and the hydrophilic edge surface [37]. However, approximately 90% of the surface area is hydrophobic [38,39]. Besides, talc carries irrelevant or no electrical charge, and the magnesium oxide layers, sandwiched between two silica layers, are electrically balanced and linked by covalent bonds. This lack of charge produces an absence of polarity in the talc particles, resulting in a non-polar and hydrophobic character, predominantly in the flat layers. As a result, talc can bind to others hydrophobic substances rather than to electrically charged materials or polar substances such as water [40].

In tests with commercial additives, the contact angle was higher than 90°, showing the hydrophobic behavior. The addition of talc particles to lubricants containing the commercial additive decreased the contact angle, showing more hydrophilic behavior. Studies have shown the adsorption capacity of talc from oily materials in aqueous [41] and

Table 2
Chemical composition, hardness, and roughness of the steel samples.

Steel	Fe (%)	C (%)	Si (%)	Mn (%)	P (%)	Hardness(HV)	Ra(μm)	Rz(μm)
SAE 1010	Balance	0.10	0.10	0.40	0.02	127(±22.5)	0.3(±0.1)	2.3(±0.3)
SAE 1045	Balance	0.47	0.15	0.50	0.02	540(±26.0)	0.3(±0.1)	2.1(±0.4)
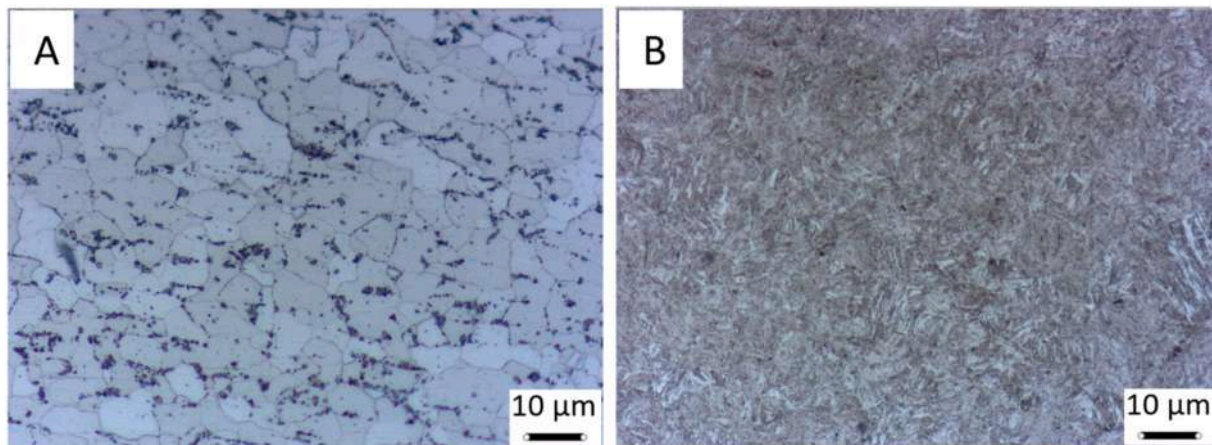
Fig. 1. Optical microstructures of the: A) normalized SAE 1010 steel, B) quenched and tempered SAE 1045 steel. Etch: Nital 3%.

non-aqueous [42] media. Considering the predominantly non-polar behavior of talc and its structure that facilitates intercalation processes, it is suggested that the presence of talc in formulations containing commercial additives promotes greater migration of organic molecules into the interior of the talc, preferentially interacting in the multiple flat layers [42]. This interaction will promote a decrease in the contact angle values, since there will be more functional groups of polar characteristics coming from the talc, and which are located on the outer edges of the talc structure (having greater affinity with water) and exposed on the surface of the film formed on the substrate. This increases the interaction of water molecules with the substrate, building H bridges of the OH groups present in the talc with water molecules. This phenomenon can also occur in lubricants containing PIL; however, this occurs less intensely, since PILs present a structure with a more polar characteristic, as shown by Alvares et al. [43], which can difficult the initial interaction with talc.

It should be noted that, after the immersion time in the lubricants, there was a significant increase in the hydrophobicity of the surfaces of the samples. According to Schmitzhaus et al. [21], the observed surface hydrophobicity can be attributed to the adsorption of ionic liquid molecules on the steel surface, which may be related to the amphiphilic character of m-2HEAOL. In this PIL, alkyl chains of the anion molecules behave in a hydrophobic way, while the head of carboxylate anion, with a polar character, behaves as hydrophilic, as well as the cationic fraction. Therefore, when comparing the lubricant containing commercial additive with m-2HEAOL, a difference in contact angle of up to 30° is observed. This decrease is related to the presence of polar groups (-OH, –COO–, –NH$_{2+}$) present in the molecular structure of m-2HEAOL, which facilitate the interaction of water with PIL.

When adding talc to the lubricant containing m-2HEAOL, a marked difference between the contact angle measurements is not evidenced, since the PIL molecule already performs sufficient interactions with water, minimizing the effect of talc on the wettability measurements.

3.2. Tribological tests

Fig. 4 shows the coefficient of friction (COF) found in the tribological tests for both steels. It is noticed that, in the beginning of the tests, the COF values decreased from 0.2 to values close to 0.1, usually in the first 250 s of the tests. After this initial transit regime, the values remained close to this order of magnitude until the end of the test, probably due to the initial surface roughness of the samples. The slight reduction is explained by the breaking of peaks present on the surface of the steel samples. Furthermore, this initial wear process and found COF levels demonstrated that a hydrodynamic lubrication mechanism is absent during the tests on both substrates. Consequently, viscosity differences of lubricants have an inconsiderable effect on the performance of the

evaluated lubricants [33] under the conditions used in this study. Due to the lubricity of the lubricants, the COF remained at a constant level until the end of the tests. No significant temperature variation was detected in the tribological system during the test.

Tests performed on normalized SAE 1010 steel showed variations in COF during the tests. These behaviors are associated with the variation in the wear scar surface throughout the test, due to the higher wear observed in the tests with this substrate (Fig. 5), mainly when analyzing the worn volume in the counterbody.

The Hersey Number (λ) was calculated by Eq. (6) [44]:

$$(\lambda) = \eta.N/P \qquad (6)$$

where η is fluid dynamic viscosity (Pa.s), N is velocity (m.s^{-1}) and P is normal load (N.m^{-1}). Both additives present in water-based lubricants (commercial additive and m-2HEAOL) contributed to a boundary lubrication regime (λ < 1) in all studied formulations [45,46]. Hsu et al. [47] comment that there are several mechanisms by which the boundary lubricating films can function like low shear interfacial lubricating layer, sacrificial layer, friction modifying layer, shear resistant layer, and load-bearing solids. In the sacrificial layer, the reaction products provide an easily removable, low shear interfacial layer against the wear track. For such films to be effective, the rate of film formation has to be higher than the rate of film removal to protect the surface [48]. In other tribological conditions, an alternative mechanism have a strongly adhered bonded layer that is shear resistant. The lubricant layer will behave as a solid exhibiting limiting shear and shear band fracture [47, 49]. As is known, this regime is independent of viscosity but is dependent on the physicochemical characteristics of the molecular film of the lubricant adhered to the surface.

ANOVA analyses confirmed the difference in performance of commercial additives and m-2HEAOL (P $_{value}$ = 0.004 < α = 0.05). Figs. 5 and 6 show the worn volumes and the wear coefficients (*k*). Despite the similarity in COF, when comparing lubricants containing commercial additive (and m-2HEAOL without the presence of particles of talc (Commercial_WP and m-2HEAOL_WP, respectively), a difference in the lubricity capacity between both additives can be seen in the tests with normalized SAE 1010 steel (values about 1.6×10^{-3} mm^3 for commercial additive against 2.4×10^{-4} mm^3 for PIL). In the case of SAE 1045 steel, the difference was unobserved, and the values for all lubricants were practically constant (about 2.0×10^{-4} mm^3).

The worn volume of the counterbodies (Fig. 5) presented values 4 orders of magnitude lower than the worn volume of the substrates. This is due to the characteristics of the ball material, which has a higher hardness (approximately 1500 HV) than the hardness of the steel alloys. Due to this low wear, no signs of Zr were detected in the EDS tests performed on the wear tracks. However, there were differences between
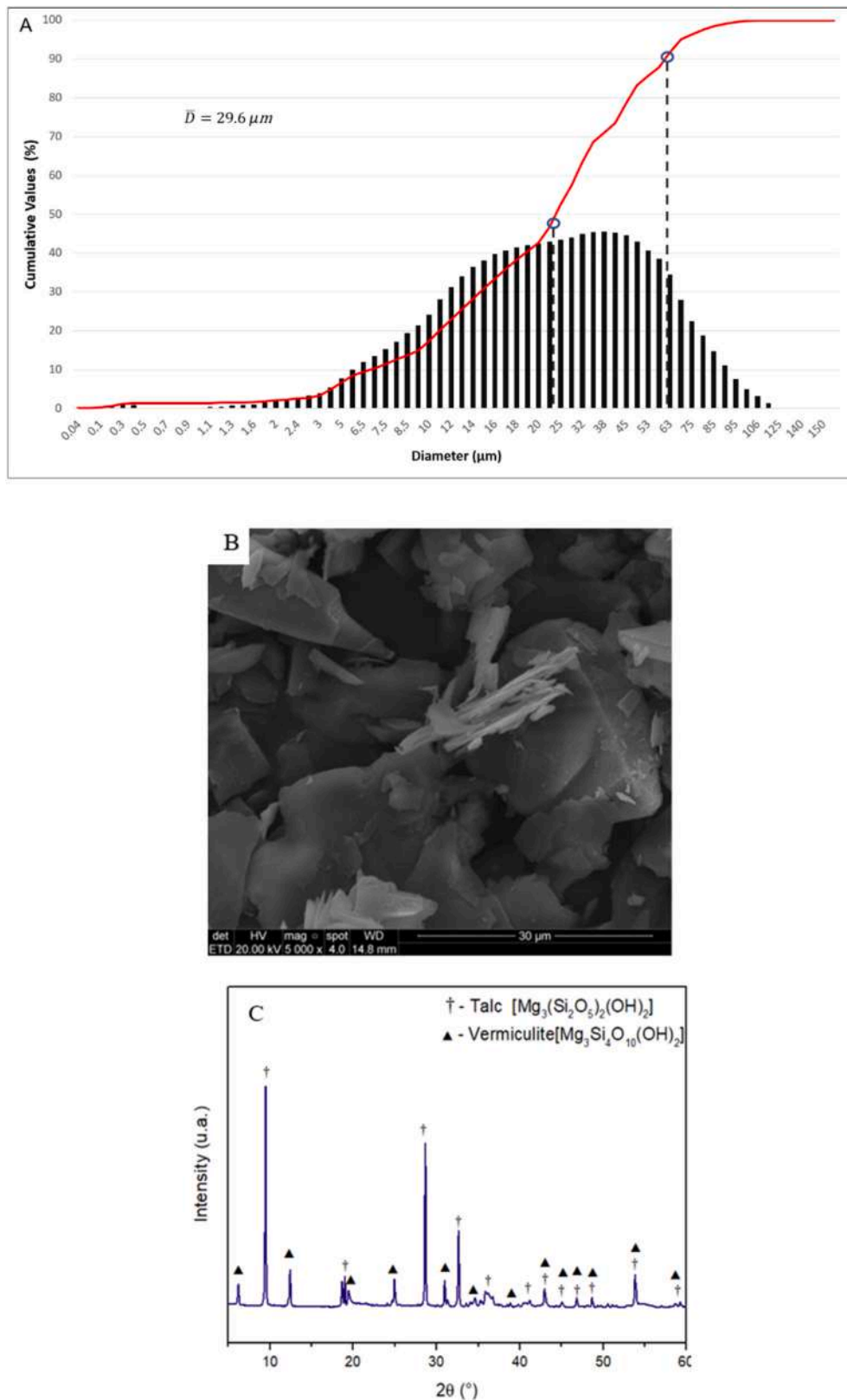
Fig. 2. Analysis of talc particles. A: Particle size distribution. B: SEM image of talc particles. C: XRD result.

the volume worn in the tests performed. Despite the hardness of the quenched and tempered SAE 1045 steel, the worn volume of the balls applied in these tests (between 1.5×10^{-7} mm^3 to 2.16×10^{-7} mm^3) showed a lower wear volume than the balls in the SAE 1010 tests (between 3.2×10^{-7} mm^3 to 4.93×10^{-7} mm^3). The higher wear in the SAE

1010 samples generated a larger ball-plate contact region compared to the SAE 1045 tests, generating a seeming higher wear scar and wear volume on these spheres. It should be noted that the method proposed by the ASTM G133-5 standard for measuring the worn volume of the spheres may have some inaccuracy between the measured values and
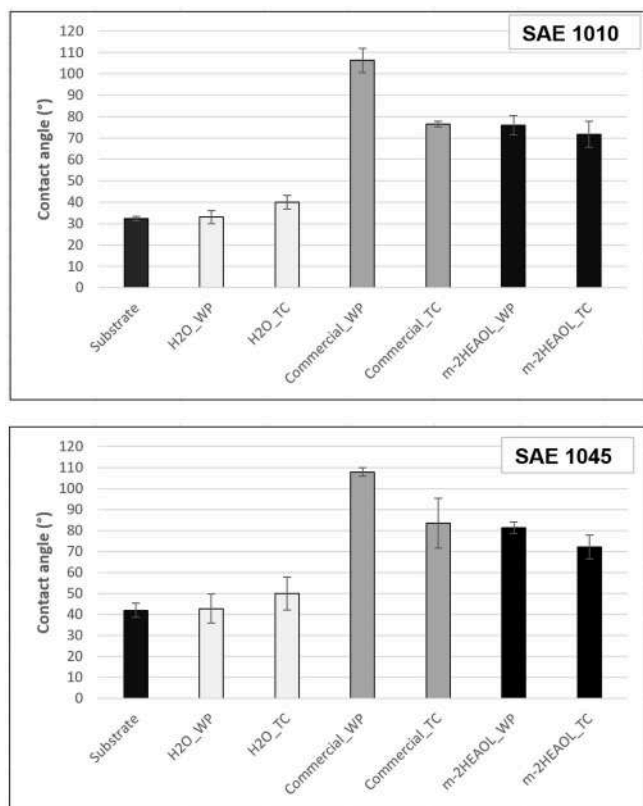
Fig. 3. Wettability after 1 h of immersion for both systems.

Fig. 4. Coefficient of friction. A: SAE 1010 lubricated with lubricants containing commercial additive and particulates; B: SAE 1010 lubricated with lubricants containing PIL and particulates; C: SAE 1045 lubricated with lubricants containing commercial additive and particulates; D: SAE 1045 lubricated with lubricants containing PIL and particulates.

the actual values. The measurement uncertainty of this technique for measuring the worn volume of the sphere was estimated using equation (5) [31], obtaining a value of around 15% of measurement uncertainty. The value varied between 13% and 17%. Despite that, it was possible to differentiate the worn volume between the tribological systems studied. Furthermore, the results were consistent with what was expected in terms of counterbody wear.

As shown in Fig. 6A and by the statistical analysis (P $_{value}$ = 0.001 < α = 0.05), the talc particle addition increased the lubricity of lubricants containing the commercial additive in the tests for SAE 1010 steel. The k coefficient increased from levels close to 4.5×10^{-5} mm^3 /Nm in the Commercial_WP lubricant, to values near 1.0×10^{-5} mm^3 /Nm in the Commercial_WP_TC_0.05 lubricant and to 0.5 $\times 10^{-5}$ mm^3 /Nm in the lubricant Commercial_WP_TC_0.1. This means that, as the concentration of particles was increased in lubricants containing the commercial additive, the lubricity increased, leading to a decrease in the k coefficient to values close to those of lubricants containing m-2HEAOL ionic liquid (Fig. 6B).

ANOVA demonstrated a synergistic effect between lubricants and talc particles (P $_{value}$ = 0.004 < α = 0.001). The synergistic effect was detected by this analysis, mainly due to the large variation of worn volume in the analyses involving normalized SAE 1010 steel with the commercial additive, as observed in Figs. 5A and 6A. Possibly, the well-known lubricating capacity of talc [19] increased the performance of lubricants containing the commercial additive, leading to a decrease in the worn volume and the k coefficient.

However, the behavior of lubricants with added m-2HEAOL (with and without talc particles) was always superior when compared with the commercial additive. The polar nature of the carboxylate anion of the PIL molecule made it difficult to interact with the non-polar talc molecule, preventing the formation of even more lubricating talc particles, as in the case of lubricants containing the commercial additive. Schmithaus et al. [21] explained that this PIL molecule is adsorbed on the metallic substrate through a mixed phenomenon of physisorption and
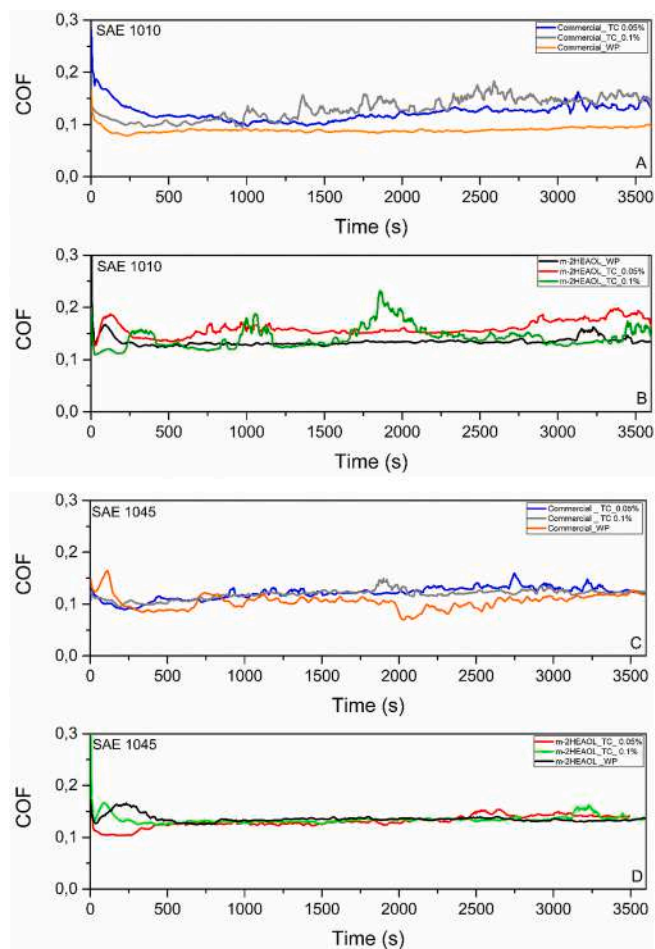
chemisorption. Chemisorption is the predominant phenomenon, i.e. steel can develop electrostatic interactions and some charges shared with PIL molecules.

Fig. 7 shows the RAMAN results of wear tracks after the tribological tests. Similar results were found off-track for both additives. The analysis detected chemical bonds present in both lubricants, i.e. there was indicating that occurred adsorption of the commercial additive and m-2HEAOL on the evaluated metallic surface. The presence of talc particles in the commercial lubricant was not evidenced by Raman analysis. The peaks identified are from the organic groups that are likely to be characteristic of the commercial lubricant. As highlighted by the manufacturer, this lubricant is water-based and silicone-free, contains organic compounds and amine salts. Fig. 7A 7C show the characteristic peaks of oxygenated organic compounds, as: C=O (670 cm^{-1}) [50], C–O (770 cm^{-1}) [51], COC (941–1050 cm^{-1}) [52], in addition to the carbon chain: CC (1062 cm^{-1}, 1251 cm^{-1}) [53,54], C=C (1555 cm^{-1}) [55], –CH$_2$ – (815 cm^{-1}) [50].

In the lubricant (containing) PIL (Fig. 7B), there is a greater amount of oxygenated organic groups: C=O, CO, COC [56], when compared to the commercial lubricant adsorbed on SAE 1010 steel. It is noteworthy that the analysis by RAMAN allows the identification of functional groups and organic molecules based on molecular vibration. In this sense, the difficulty in finding characteristic peaks of talc molecules in lubricants may be associated with the absence of covalent bonds formed between the lubricants and the particles. In this case, the talc particles
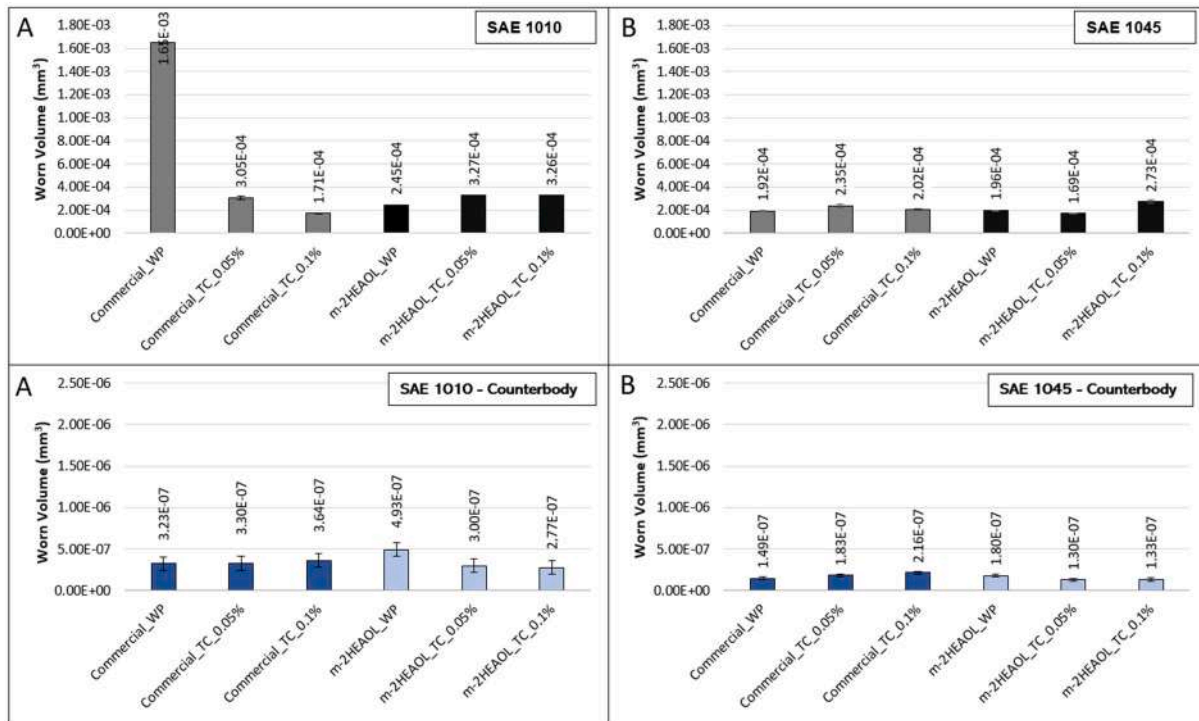
Fig. 5. Comparison between the worn volume after the tribological tests: A) normalized SAE 1010 steel, B) quenched-tempered SAE 1045 steel.
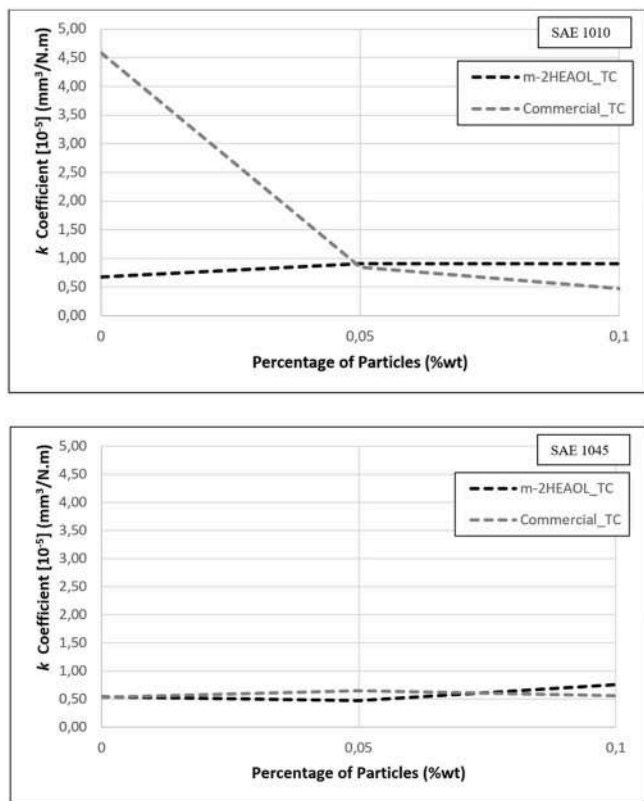
Fig. 6. Coefficient k for water-based lubricants, as a function of wt % of talc for lubricants with the addition of PIL (m-2HEAOL) or commercial lubricant.

were likely mixed with the lubricants without the formation of a strong interaction through the formation of primary bonds.

According to Xiao et al. [57], the lubrication mechanism of ionic liquids, in the limit lubrication regime, can form strong adsorption films on the friction surfaces, due to the polarity of the ILs, leading to a reduction in wear. Longer alkyl chains in IL cations, such as those present in m-2HEAOL molecules and detected in the RAMAN analysis (Fig. 7B–D), are more favorable to form thick films due to van der Waals forces. It is known that the main lubrication mechanism of ionic liquids is by adsorption, which is a key factor for lubrication [58]. As suggested by Kondo [59], two factors determine the improvement in lubricity generated by PILs: better coverage and strong interaction between the lubricant and the metallic surface. The best coverage is attributed to the balance of both hydrophobic and hydrophilic properties of the lubricant. The balance between these properties is achieved when the hydrocarbon chain is introduced. The results found by Huang et al. [60] indicated that the strong adsorption of cations played an important role in the lubricity of the lubricants studied by these authors. Furthermore, there is a great advantage in the adsorbed layer of PIL in relation to the commercial additive, detected in the RAMAN analysis and previously reported, which makes the interaction between the tribofilm and the newly worn surface increases the performance of the lubricant. The anionic portion of the ionic liquid can be easily adsorbed onto the positively charged locations of the metal worn surface, providing protection against severe wear. Therefore, under adverse slip conditions, active elements in ionic liquids can react with the worn surface, forming a reaction film on the freshly worn surface of the material [61].

Fig. 8 demonstrates the differences found in the wear tracks of the tests lubricated with lubricants added with PIL and 0.1% talc particles on both substrates. The different colours are a result of phenomena that occurred between the wear track surface under conditions of boundary limit lubrication (tribochemical reaction), as suggested by Hsu et al. [62]. Friction can induce complex surface changes on the worn surface such phase transitions, material transfer, oxidation, plastic deformation.
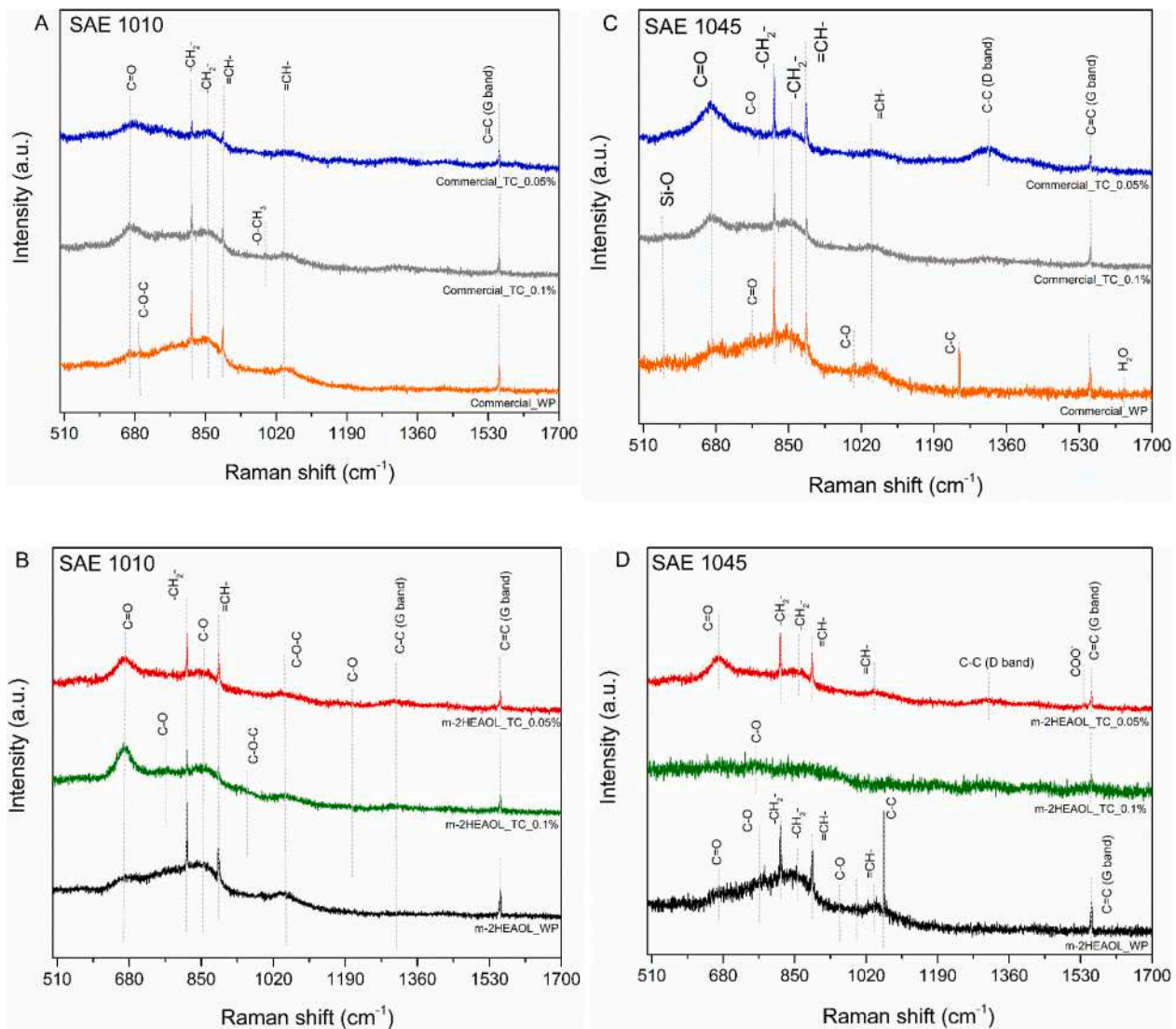
Fig. 7. RAMAN analyses on wear tracks (wavelength of 532 nm). A: SAE 1010 with commercial additive; B: SAE 1010 with m-2HEAOL additive; C: SAE 1045 with commercial additive; D: SAE 1045 with m-2HEAOL additive.

The cooperation between thermal, chemical, and mechanical effects may be responsible for these surface changes [63]. The tribolayer formed by oxides and material of both counterfaces and their oxides are called mechanically mixed layer [64,65]. The RAMAN analysis, using the laser beam with a wavelength of 632.8 nm [66], permits identification of oxides formed in wear tracks on steel substrates. In all tracks, iron oxides were detected (α-Fe_2O_3- hematite and Fe_3O_4 – magnetite). In the reciprocating sliding tests, α-Fe_2O_3 oxides is rarely formed in lubricated tests, unless oxygen is present in the lubricant [67]. This is the case of the water-based lubricants applied in this study. It is known that FeO_3 and Fe_3O_4 are hard and brittle oxides and could supress deformation, under certain conditions [68]. Crockett et al. [69] reported the formation of oxide films composed of magnetite and hematite in lubricated HFRR tests using different additives in commercial diesel. According to the authors, the increase in the wear resistance in the tested tribological conditions caused by hematite was practically insignificant. Although, the formation and preservation of hematite in the wear track are associated with tribological systems with low wear. Therefore, the homogeneous oxide film found in the wear track in the m-2HEAOL tests on SAE 1045 steel confirms the lubricity of the adsorbed PIL film detected in Fig. 7D.

Magnetite and Hematite are known Fe oxides formed by corrosion

[69]. In addition, these oxides are also associated with high temperatures, and can be formed by the tribooxidation sub mechanism during wear tests [24,70]. According to Quinn [67], these oxides may be formed at the "hot-spot" temperature in the real contact areas, even in a lubricated tribological systems. The higher wear resistance of SAE 1045 steel, contributed to the elevation of the hot-spot temperatures between the surface and the zirconia ball. Depending on speed, the mechanical dissipation of friction produces heat which raises the temperature at the contact asperities substantially for a microsecond or less [47]. Nonetheless, compared with dry wear, frictional temperatures in lubricated wear are much lower and the presence of oil, or water-based lubricant, may limit or prevent oxide film growth [68]. In the adsorption of PIL on SAE 1045 steel (Fig. 7D), the presence of oxygenated organic groups was not identified by RAMAN analysis but those characteristic groups of the lubricant's own carbon chain (CH, –CH_2 -, =CH-, CC). However, the wear tests performed on the SAE 1045 showed very similar *k* values (Fig. 5) in all measurements performed, i.e. similar performances.

Furthermore, it is known that the oxide formed by tribochemical reaction remains stable from a critical thickness [70]. The lower lubricity of the lubricants containing the commercial additive, even in the tests containing talc, prevented the formation of the homogeneous oxide film, which were removed during the test on both substrates. The lower
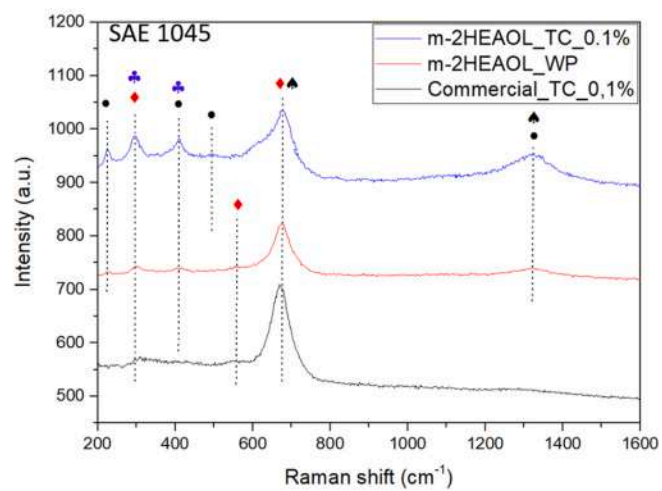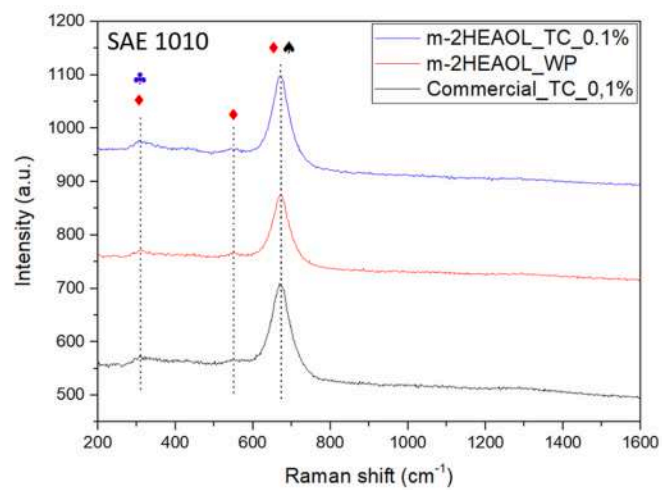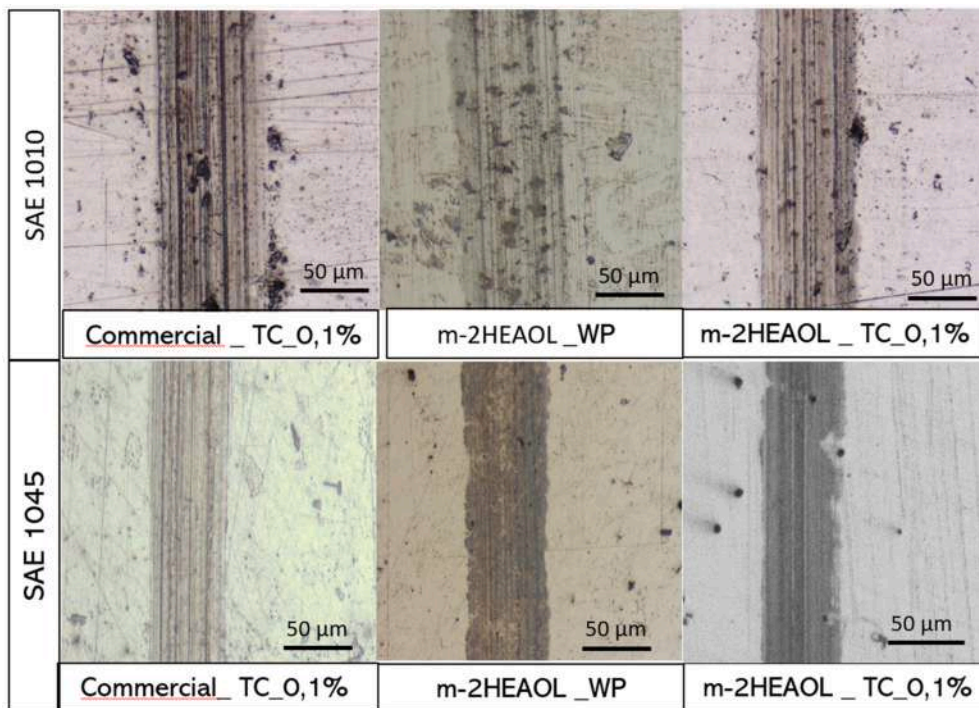
Fig. 8. Optical microscopy and RAMAN (wavelength of 632.8 nm) analysis on m-2HEAOL wear tracks. Where $\bullet = \alpha - Fe_2O_3$ (hematite), $\blacklozenge = Fe_3O_4$ (magnetite), $\clubsuit = \alpha - FeOOH$ (goetite), $\spadesuit = \gamma - FeOOH$ (lepidocricite).

wear resistance of SAE 1010 steel also prevented the formation of this homogeneous film in all lubricants. Thus, in all tests of SAE 1010 steel and in tests of lubricants with commercial additive in SAE 1045 steel, only oxide islands were detected in the worn tracks (Fig. 8). However, as the lubricants used in the study are water-based, hydrated oxides (as $\alpha - FeOOH$ and $\gamma - FeOOH$) can also be associated with peaks at the same wavelength numbers (298, 397, 414, 1322 cm^{-1}) [71,72].

Figs. 9 and 10 show the SEM analyses of wear tracks with lubricants on both substrates. It is observed that all tests showed abrasive wear lines aligned with the sliding direction [73]. The micro-cutting/micropluging (groves) are the main abrasive micro-mechanisms [70,73,74]. In commercial additive and PIL wear tests, delamination (a submechanism of surface fatigue with predominantly plastic interactions) were found in both substrates (Figs. 9A–10A) [24]. Observing the wear track surfaces of SAE 1010 steel with the Commercial_WP lubricant (Fig. 9A), the severity of plastic deformation and micropluging is noted. The addition of talc caused a decrease in the severity of wear (Fig. 9B) in the tests containing commercial additive, caused mainly by abrasive wear, (microcutting/micropluging). As for the behavior of lubricants containing PIL (Fig. 9C–D), the higher lubricity of this additive led to less intense formation of abrasive wear mechanism and sub-mechanism, demonstrating the superior lubricity of m-2HEAOL in relation to the commercial additive. However, circular craters (pits) generated by the cyclic stresses inherent to the applied

wear test were found, mainly in tests containing talc particles (Fig. 9D).

Although the behavior of the COF and the worn volume were similar in all tribological analyses of SAE 1045 steel, differences in the wear dynamics in the tests with different lubricants can be observed. SEM images of the wear track with Commercial_WP lubricant (Fig. 10A) showed a higher severity compared to the other tests. Regions with plastic deformation, probably caused by micropluging, were detected, in addition to delamination [24]. The worn volume was similar in the tests with the Commercial_WP and the Commercial_TC lubricants. However, the addition of talc reduced the severity of wear in the quenched and tempered SAE 1045 steel (Fig. 10B) when compared to SAE 1010 steel. SEM images of in the tests using m-2HEAOL_WP detected groves resulting from abrasive wear, however, with a lower severity than Commercial_WP. Regions with deformation were also not detected, indicating that microcutting was the main active submechanism in this tribological system. Guo et al. [45] also demonstrated that tests lubricated with PILs could mitigate the occurrence of plastic deformation that other lubricants were incapable. In the wear tracks, those lubricants containing PILs also showed grooves associated with abrasive wear in a borderline lubrication regime. However, as seen in Fig. 10D, the addition of talc particles caused the formation of regions with plastic deformation and pits generated by surface fatigue (indentations). Thus, the lubricity of m-2HEAOL is superior to talc particles. Therefore, the addition of particles impaired the adsorbed layer of this additive, which
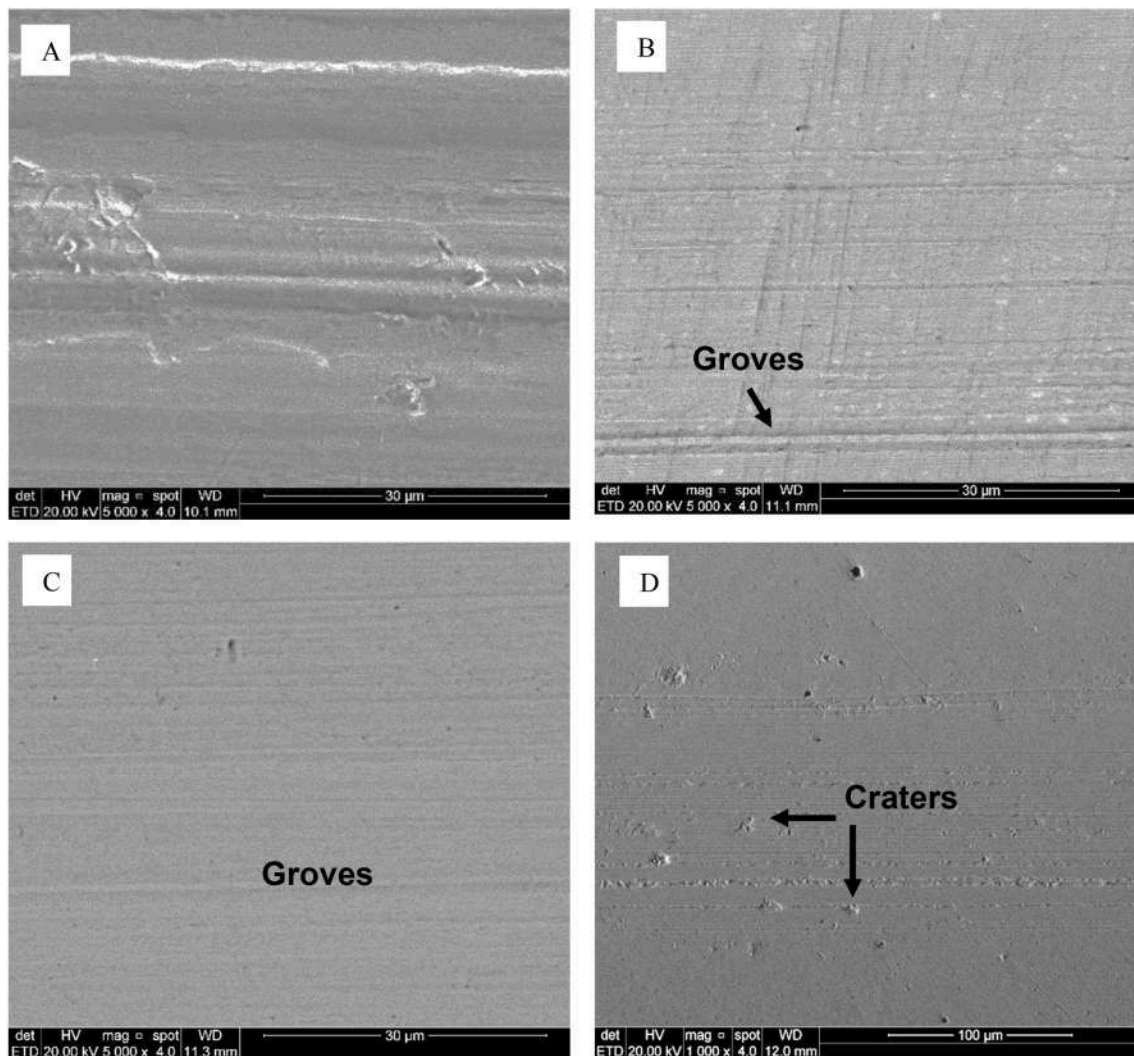
Fig. 9. SEM Images: A: SAE 1010 with Commercial_WP; B: SAE 1010 with Commercial and 0.1% TC C: SAE 1010 with m-2HEAOL_WP; D: SAE 1010 with m-2HEAOL and 0.1% TC.
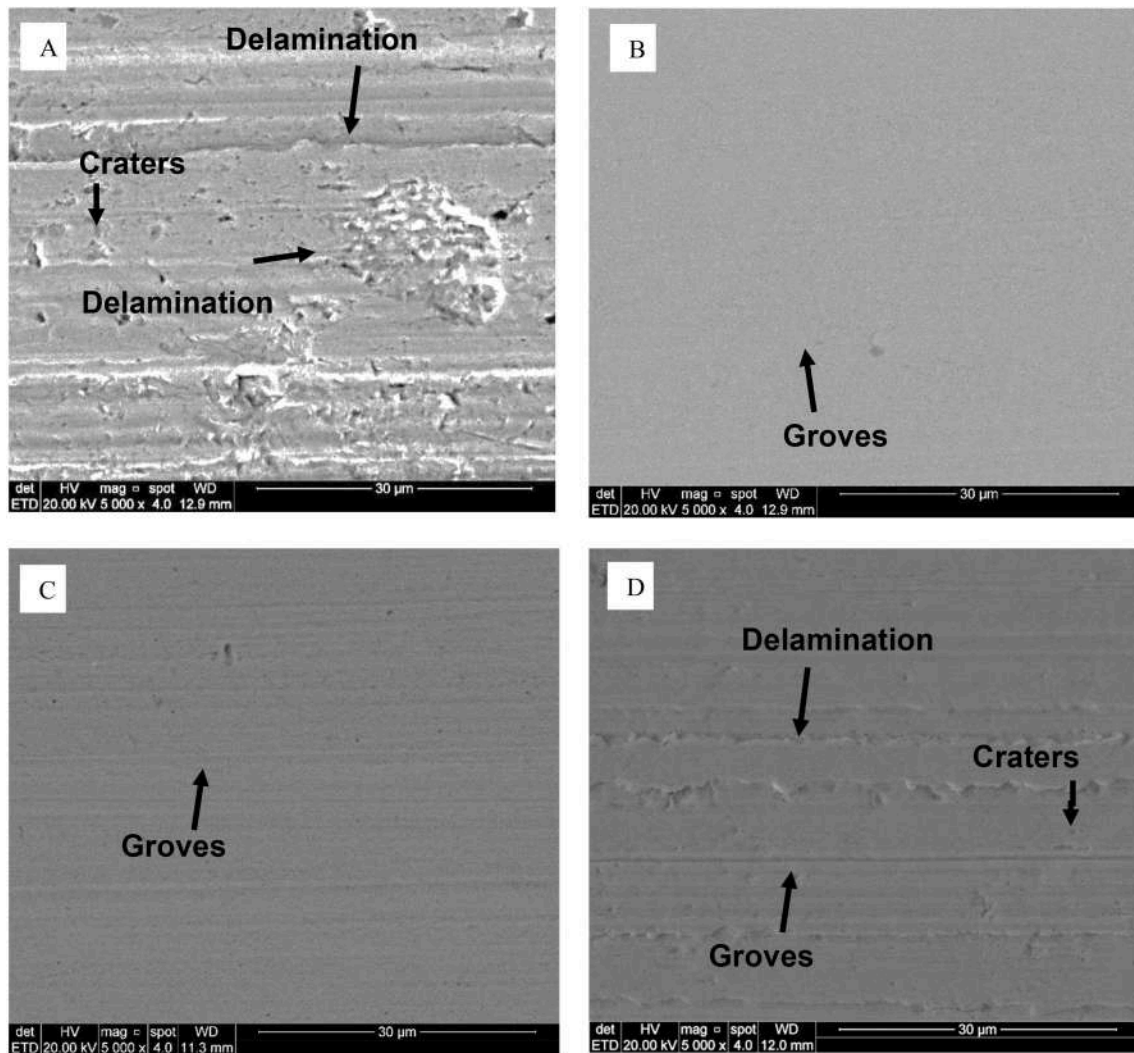
Fig. 10. SEM Images: A: SAE 1045 with Commercial_WP; B: SAE 1045 with Commercial and 0.1% TC C: SAE 1045 with m-2HEAOL_WP; D: SAE 1045 with m-2HEAOL and 0.1% TC.

led to the occurrence of plastic deformation and surface fatigue, which were not detected in the tests without particles.

Figs. 11 and 12 show the results found in the zirconia balls used in the wear tests. The EDS analyses detected the presence of Fe at the contact point of the ball with the substrate, possibly associated with the removal of Fe oxides detected in Fig. 9. However, a higher amount of material adhered to the sphere can be seen in systems lubricated with the commercial lubricant, as observed in Figs. 11A and 12A. Besides, optical and SEM images show the presence of groves on the surface of the balls, which indicates microcutting and/or micromining (abrasion submechanisms) [24]. Even with this wear, EDS analysis of the wear tracks did not detect the presence of zirconium. The balls used in the tests of SAE 1045 steel (Fig. 12E) lubricated with PIL showed a lower amount of material adhered to the surface. EDS analysis (Fig. 12 F) detected mainly Zr peaks. Possibly, the oxide layer formed in these tribological systems prevented the wear of the tracks and, consequently, the adhesion of this worn material to the spheres.

3.2.1. Discussion

Despite having similar COFs, lubricants containing m-2HEAOL and commercial additive, applied to SAE 1010 steel, presented different lubrication mechanisms. The characteristics of the PIL molecule induce to the formation of a high lubricity tribofilm, reducing the worn volume (Fig. 5) and the specific wear rate k (Fig. 6), and significantly mitigating

the occurrence of wear adhesive and plastic deformation in relation to the performance of the commercial additive. Due to the higher lubricity of PIL in the borderline lubrication regime, talc particles practically unchanged the lubricity behavior of the PIL, and this can be attributed to the oxides formed by tribochemical reaction, which did not reach the critical thickness, and can be removed during the test. Despite the formation of an adsorbed layer in lubricants containing a commercial additive, their lubricity was substantially lower than that of PIL tribofilm. Therefore, the addition of talc particles led to a reduction of the k coefficient to levels close to that of the m-2HEAOL_WP lubricant for SAE 1010 steel. In addition, the oxide layer formed in quenched and tempered SAE 1045 steel in the PIL lubricated tests may also have contributed to the increased wear resistance of these tribological systems. The presence of hematite may demonstrate the superior lubricity of PIL, as previously mentioned. In these tests, a tribofilm composed by two layers was formed: the oxide layer and the adsorbed layer, as proposed by Stemmer and Fischer [24]. Unlike other systems, this oxide film made it difficult for material to adhere to the wear sphere, as evidenced by the EDS analysis.

According to Hsu and Gates [47], for an ideal boundary lubricating film, a strongly bound molecule, as in the case of the studied PIL, could provide a softer and more deformable component of the film that would distribute the roughness load. Furthermore, it could provide an easily shear layer to limit surface stress penetration. This ability of m-2HEAOL
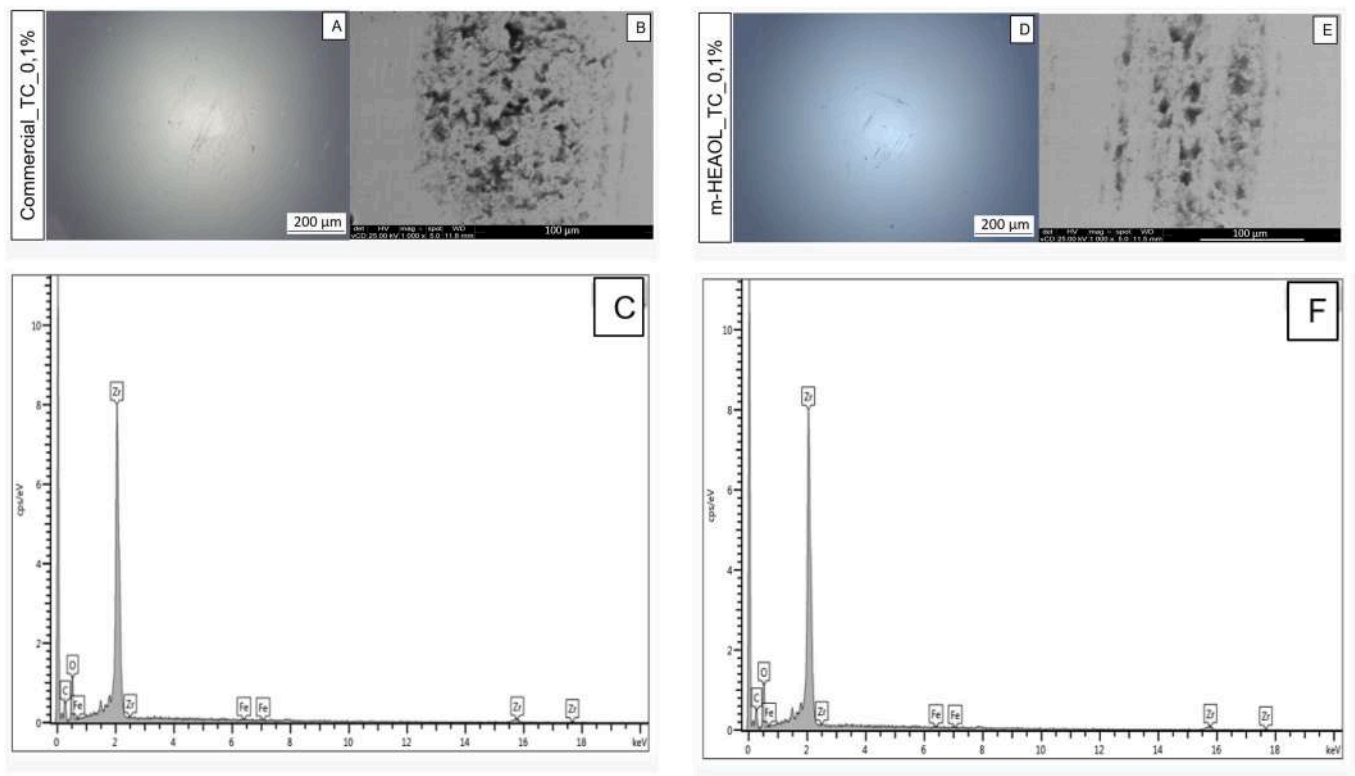
Fig. 11. Images of the spheres of SAE 1010 analyses. A, D: Optical microscopy; B, E: Scanning electron microscopy (SEM); C, F: EDS analysis.
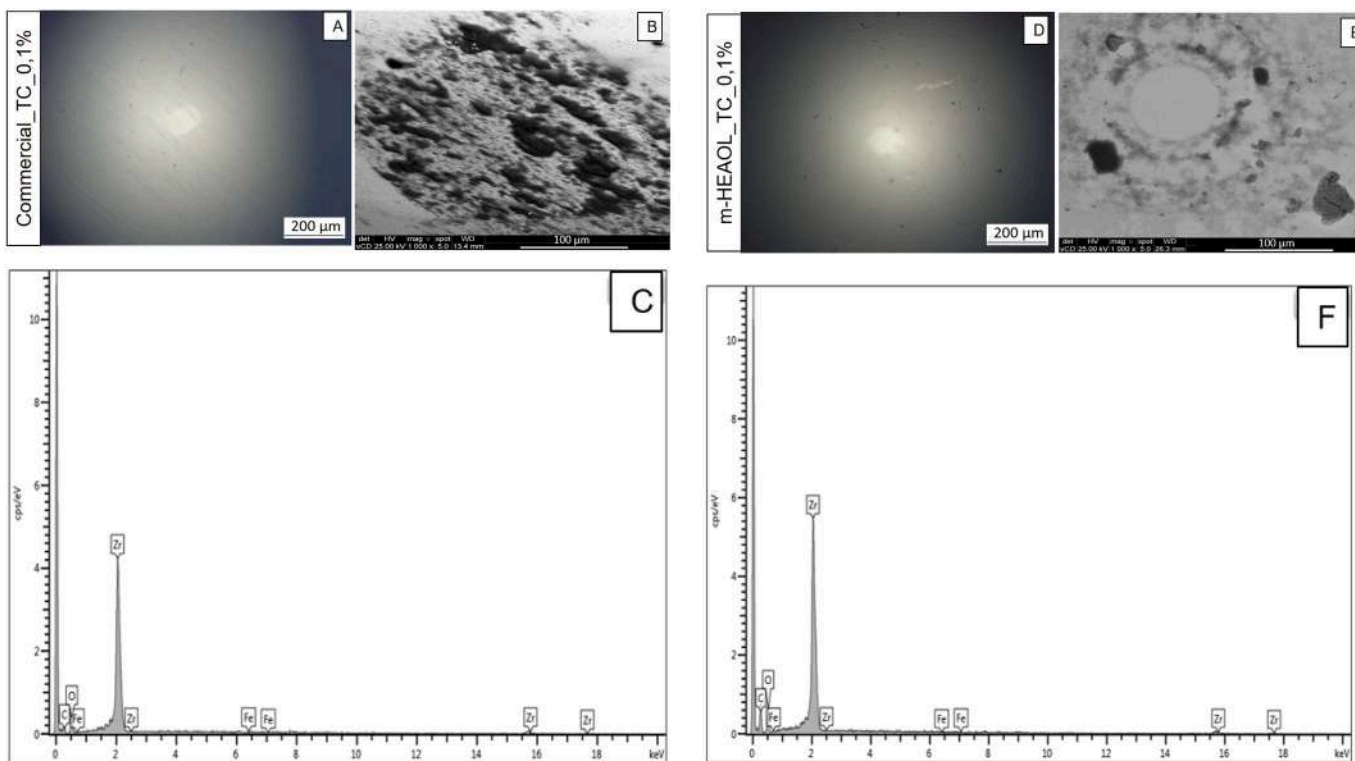
Fig. 12. Images of the spheres of SAE 1045 analyses. A, D: Optical microscopy; B, E: Scanning electron microscopy (SEM); C, F: EDS analysis.

was present in all tests carried out with lubricants containing this additive. These authors also comment that boundary lubricating films can be thought of as a mixed component film composed of a hard load-bearing phase and a soft, easily sheared phase. This hard phase was

formed in tests lubricated with PIL on quenched and tempered SAE 1045 steel, through tribochemical reactions, possibly by thermal action. Therefore, in the tribological tests of this steel, the adsorption capacity of the PIL and the tribochemical reactions favored the formation of an

ideal limit lubrication regime, which, together with the greater wear resistance of this material, significantly reduced the wear volume in all formulations containing m -2HEAOL.

The balls used in all tests wore 10,000x less than the metallic substrates and Zr were not detected in the EDS tests. Microcutting/micropluging (Abrasive Wear) were the main wear sub mechanisms detected in all tracks. Furthermore, delamination (surface fatigue) and craters were also detected. The proposed mechanisms are exemplified in Fig. 13.

3.3. Electrochemical tests

In order to analyze the corrosivity of the studied lubricants, polarization curves were performed on samples of both steel alloys in lubricants containing m-2HEAOL and commercial additive, with and without 0.1% talc particles (%wt.). Tests in deionized water without particles (H$_2$O_WP) and containing 0.1% (%wt.), H$_2$O_TC, were also performed.

The results are shown in Fig. 14. Analyzing the curves of SAE 1010 steel, it can be seen that the curves with electrolyte composed of H$_2$O, with or without talc particles in relation to the curves with lubricants, showed an abrupt increase in current density (at an approximate potential of 300 mV$_{SCE}$) indicating a greater acceleration in the corrosive process above this potential. However, even at free potential, the current values already refer to a very high corrosion rate in the H$_2$O_TC formula, behavior that was not observed in the curves with commercial additive and PIL. The curves with commercial additives and m-2HEAOL, from potentials close to 300 mV$_{SCE}$ with and without the presence of talc particles, showed a pseudo passivation, which may be associated with the adsorption of PIL and commercial additive, as demonstrated by

RAMAN analysis (Fig. 7) on the SAE 1010 steel surface. The corrosion potentials presented in Table 4 stabilized at −230 mV$_{SCE}$ and −260 mV$_{SCE}$ with electrolyte H$_2$O_WP and H$_2$O_TC, respectively. However, in the presence of PIL, they shifted to more positive potentials between −155 mV$_{SCE}$ and −187.5 mV$_{SCE}$ and between −141 mV$_{SCE}$ and −165 mV$_{SCE}$ in lubricants containing commercial additive, indicating a better behavior in relation to corrosion in the presence of the additives. The corrosion current densities in the tests for this steel remained at levels close to 10^{-2} μA/cm^2, with a slightly lower value for the tests in the lubricant Commercial_WP, with a current density of 0.7×10^{-2} μA/cm, and this was reflected in the lower corrosion rate (0.8 mm/year). In the other tests for the SAE 1010 steel, a very similar corrosion inhibition capacity can be seen between the commercial additive and PIL. There was a decrease in the Corrosion Rate, to values similar for both additives.

The H$_2$O tests for SAE 1045 quenched and tempered steel showed a higher reactivity than SAE 1010 steel, taking the corrosion rates to higher values, where H$_2$O_WP presented a corrosion rate of 11.4×10^{-4} mm/year. As can be seen in Fig. 15, after the electrochemical test, the SAE 1045 steel sample in the H$_2$O_TC electrolyte showed pronounced pitting and red corrosion product. Other authors have demonstrated the influence of microstructure on the corrosion resistance of steels. Katyar et al. [75] demonstrated that the martensite obtained by quenching was the microstructure with the greatest tendency to corrosion compared to other pearlitic and bainitic structures. The results in Clover et al. [76] also showed that the martensitic microstructure had the highest corrosion rate among the analyzed microstructures. As can be seen in Fig. 14, for SAE 1045 steel in the presence of the H$_2$O_TC electrolyte, the curve shows a shift to higher current densities compared to the H$_2$O_WP
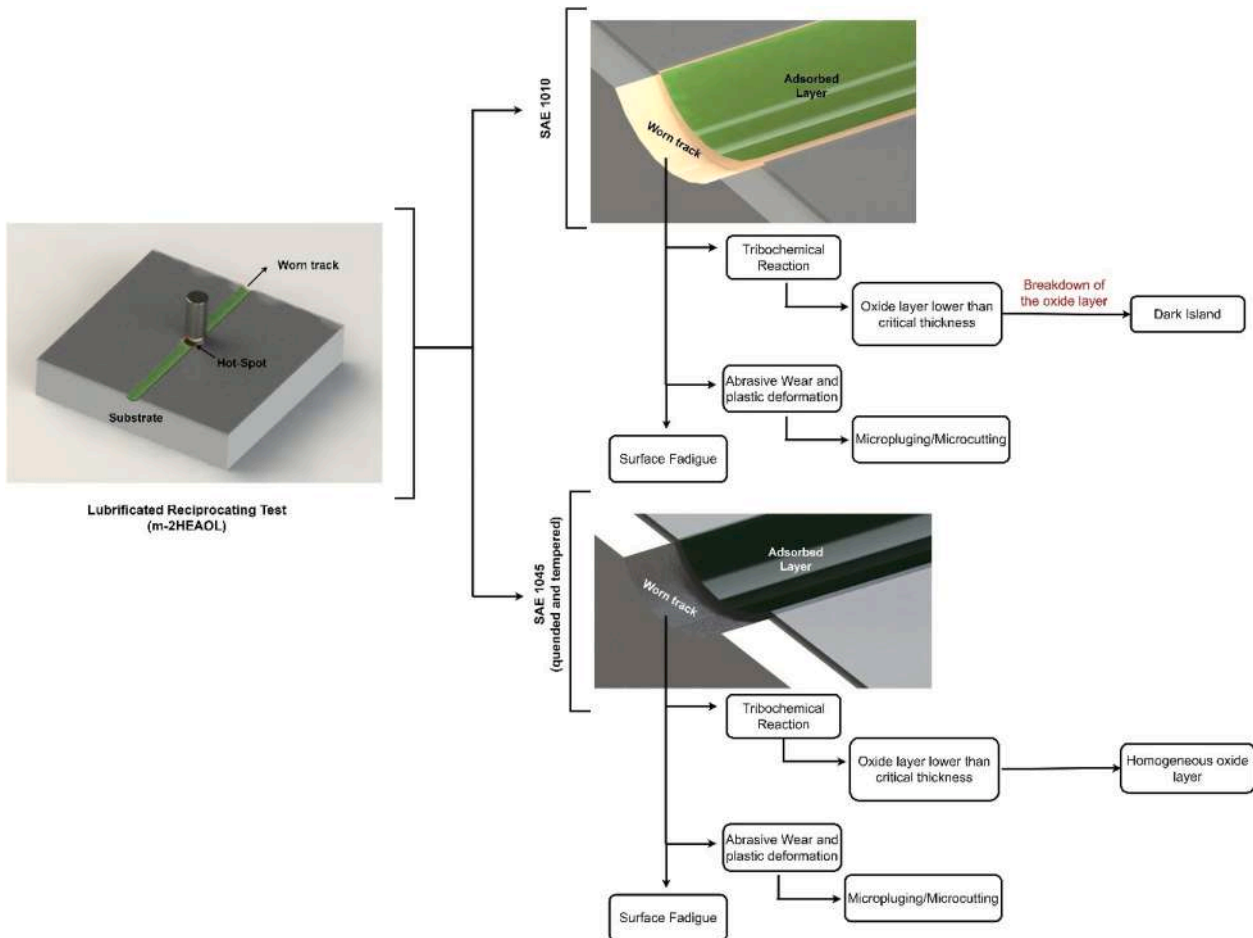
Fig. 13. Representation of the lubrication mechanisms of the m-2HEAOL lubricants.
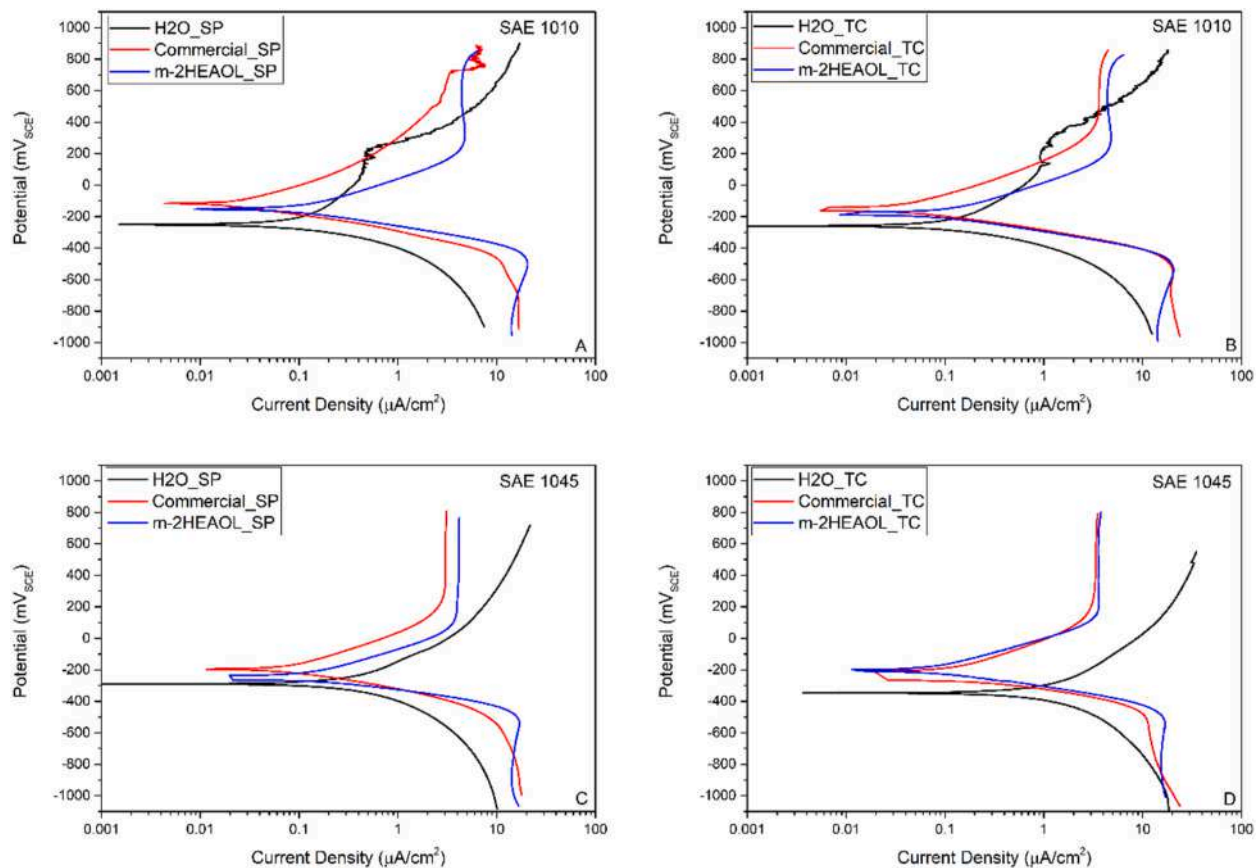
Fig. 14. Potentiodynamic polarization curves. A: SAE 1010 with lubricants without talc particles; B: SAE 1010 with lubricants containing 0.1% (wt.%) talc particles; C: SAE 1045 quenched and tempered with talc-free lubricants; D: SAE 1045 quenched and tempered with lubricants containing 0.1% (wt.%) talc particles.

Table 4
Electrochemical results obtained from Tafel extrapolation.

Lubricant	Substrate	E_{corr} (mV$_{SCE}$)	$i_{corr}[10^{-2}]$ (μA/cm^2)	$Rp[10^5]$ (Ω/cm^2)	Corrosion Rate $[10^{-4}]$ (mm/ano)
H$_2$O _WP	SAE 1010	−230 (29.0)	3.50 (0.7)	14.5	4.0
H$_2$O _TC		−260 (25.0)	5.00 (2.0)	7.4	5.7
m-2HEAOL_WP		−155 (7.0)	1.50 (0.7)	19	1.7
m-2HEAOL_TC		−187.5 (3.0)	3.50 (2.0)	8.0	4.0
Commercial_WP		−141 (13.0)	0.7 (1.5)	49	0.8
Commercial_TC		−165 (21.0)	3.50 (2.0)	8.0	4.0
H$_2$O _WP	SAE 1045	−305 (21.0)	10.00 (0.5)	3.1	11.4
H$_2$O_TC		−330 (14.0)	26.50 (20.0)	0.3	30.3
m-2HEAOL_WP		−230 (28.0)	6.50 (0.7)	3.4	7.4
m-2HEAOL_TC		−180 (70.0)	7.00 (3.0)	5	8.0
Commercial_WP		−220 (42.0)	2.00 (0.5)	15	2.3
Commercial_TC		−255 (7.0)	8.00 (1.5)	2.3	9.1

electrolyte and, also, the curves with the other additives (E $_{Corr}$ = −330 mV$_{SCE}$ and I$_{Corr}$ = 26.50 μA/cm^2). Consequently, it has the highest corrosion rate among the systems studied (CR = 30.3 × 10 $^{-4}$ mm/year).

The H$_2$O_TC had a pH close to neutral (pH = 7.5), which should not contribute to the corrosive process, since in the presence of water without talc we would have a pH close to it. The XRD analysis, as mentioned above, detected only magnesium silicate hydroxide phases (Fig. 2C), suggesting that the increase in the corrosive process was not caused by contamination by corrosive substances, such as chloride, for example.

It is known that, in some situations, talc can induce increased corrosion. Dubus et al. [77] showed that talc particles in the atmosphere of museums can lead to increased corrosion when deposited on metallic surfaces, due to the adsorption of humidity from the air by these particles. This difference in humidity leads to the formation of corrosion by differential aeration. Possibly, talc caused an increase in the corrosion rate (CT) in a similar way, even with the differences in humidity in the environment between the two studies. As shown in previous works [15, 34], and in section 3.1, particles in a solution with sizes larger than 0.5 μm tend to prevent a stable suspension, depositing on the surface. The talc particles used as an additive had an average size of 23.7 μm. Thus, these deposited particles would generate a corrosion process by differential aeration or crevice, leading to the formation of the type of corrosion found on the steel surface (Fig. 15). Due to the reactive nature of the quenched and tempered SAE 1045 steel discussed above, this phenomenon occurred more intensely in this substrate.

However, in lubricants used as electrolytes containing commercial additives and PIL, in SAE 1045 steel, this increase in the corrosivity of talc particles was mitigated in relation to electrolytes with talc, but without the commercial additives and m-2HEAOL, resulting in much smaller rates of corrosion: m-2HEAOL_TC (CT = 8.0 × 10^{-4} mm/year) and Commercial_TC (9.1 × 10^{-4} mm/year). However, the corrosion rates found for lubricants with talc gave values higher than the rates found for additives without talc, in both substrates (Table 4). Therefore,
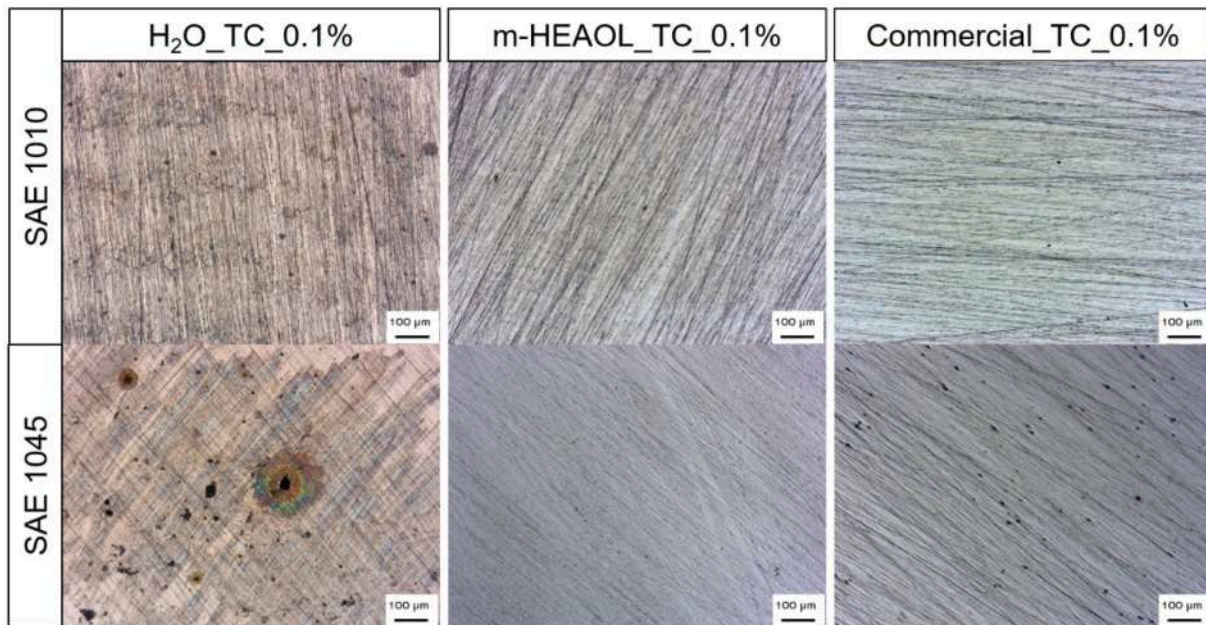
Fig. 15. Images obtained by optical microscopy of the surface of the samples after electrochemical testing.

the adsorption mechanism described above, involving commercial additive and talc, contributed to the decreased corrosivity. However, the presence of talc generates a considerable increase in the corrosion rate, even in the presence of other additives. Thus, talc particles contributed to the increase in the corrosive process in all lubricants; however, the corrosion mechanism in lubricants containing m-2HEAOL was mitigated in relation to the lubricant H$_2$O_TC, due to the strong adsorption of functional groups present in the strongly polar molecule of PIL, following the model proposed by Schimtzhaus et al. [21].

4. Conclusions

In the present study, the effect of talc particles on water-based lubricants with protic ionic liquid (PIL) was investigated. The results were compared with similar formulations containing a commercial water-soluble additive. The tests aimed to evaluate the tribological and electrochemical performance of these lubricants. The main results are presented.

- In the wear tests, lubricants containing PIL showed the best performance in the formulation without talc particles, compared to the commercial ones tested for normalized SAE 1010 steel. This was due to the presence of a tribofilm formed due to the strong PIL/substrate interaction.
- SAE 1045 steel (quenched and tempered) exhibited small and uniform wear in the presence of all tested lubricants. In the case of m-2HEAOL lubricant, the formed oxide hard layer and the soft adsorbed m-2HEAOL layer, in the boundary lubricant regime, increased the wear resistance.
- The synergistic effect detected by ANOVA in increasing the lubricity of formulations containing commercial additive and talc particles led the worn volume, in tests on SAE 1010 steel, to levels similar to those of m-2HEAOL_WP (without particles), demonstrating the superior lubricity of m -2HEAOL.
- The corrosive action of talc seems to be related to the deposition of particles on the steel surface, developing a corrosion process by differential aeration. SAE 1045 steel showed a greater susceptibility to corrosion than SAE 1010 steel in all of the tested lubricants.
- PIL and the commercial additive significantly mitigated the corrosive effect generated by talc particles observed in water on both

substrates. Furthermore, the pseudo passivation observed in the potentiodynamic polarization curves was confirmed by the PIL adsorption detected by the RAMAN analysis.

Credit author statement

Victor Velho de Castro: Conceptualization; Data curation; Formal analysis; Investigation; Methodology; Writing – review & editing. Leonardo Moreira dos Santos: Data curation; Formal analysis; Investigation, Writing – review & editing. Leonardo Marasca Antonini: Investigation; Writing – review & editing. Roberto Moreira Schroeder: Data curation; Formal analysis; Investigation; Supervision; Validation; Writing – review & editing. Silvana Mattedi: Supervision; Writing – review & editing. Klester S. Souza: Investigation, Supervision; Writing – review & editing. Marcelo Barbalho Pereira: Investigation, Supervision; Writing – review & editing. Sandra Einloft: Supervision; Writing – review & editing. Carlos Alexandre dos Santos: Supervision; Writing – review & editing. Célia de Fraga Malfatti: Conceptualization; Data curation; Formal analysis; Investigation; Methodology; Project administration; Supervision; Validation; Visualization; Writing – review & editing.

Declaration of competing interest

The authors declare that they have no known competing financial interests or personal relationships that could have appeared to influence the work reported in this paper.

Data availability

Data will be made available on request.

Acknowledgements

References

[1] M.H. Rahman, H. Warneke, H. Webbert, J. Rodriguez, E. Austin, K. Tokunaga, D. K. Rajak, P.L. Menezes, Water-based lubricants: development, properties, and performances, Lubricants 9 (2021) 73, https://doi.org/10.3390/lubricants9080073.

[2] A. Tomala, A. Karpinska, W.S.M. Werner, A. Olver, H. Störi, Tribological properties of additives for water-based lubricants, Wear 269 (2010) 804–810, https://doi.org/10.1016/j.wear.2010.08.008.

[3] M. Rojas-Campanur, J. Lara-Romero, F. Chiñas-Castillo, G. Alonso-Nuñez, Tribological performance of rosin acid additives in water based lubricants, Tribol. Online 2 (2007) 29–33, https://doi.org/10.2474/trol.2.29.

[4] G.W. Stachowiak, A.W. Batchelor, Engineering Tribology, third ed., Elsevier Butterworth-Heinemann, Amsterdam; Boston, 2005.

[5] M. Akbulut, Nanoparticle-based lubrication systems, J. Powder Metall. Min. 1 (2012), https://doi.org/10.4172/2168-9806.1000e101.

[6] A. Khan, R. Gusain, M. Sahai, O.P. Khatri, Fatty acids-derived protic ionic liquids as lubricant additive to synthetic lube base oil for enhancement of tribological properties, J. Mol. Liq. 293 (2019), 111444, https://doi.org/10.1016/j.molliq.2019.111444.

[7] R.L. Vekariya, A review of ionic liquids: applications towards catalytic organic transformations, J. Mol. Liq. 227 (2017) 44–60, https://doi.org/10.1016/j.molliq.2016.11.123.

[8] M. Watanabe, M.L. Thomas, S. Zhang, K. Ueno, T. Yasuda, K. Dokko, Application of ionic liquids to energy storage and conversion materials and devices, Chem. Rev. 117 (2017) 7190–7239, https://doi.org/10.1021/acs.chemrev.6b00504.

[9] K.S. Egorova, E.G. Gordeev, V.P. Ananikov, Biological activity of ionic liquids and their application in pharmaceutics and medicine, Chem. Rev. 117 (2017) 7132–7189, https://doi.org/10.1021/acs.chemrev.6b00562.

[10] H. Liu, H. Yu, Ionic liquids for electrochemical energy storage devices applications, J. Mater. Sci. Technol. 35 (2019) 674–686, https://doi.org/10.1016/j.jmst.2018.10.007.

[11] C.S. Madankar, S. Pradhan, S.N. Naik, Parametric study of reactive extraction of castor seed (Ricinus communis L.) for methyl ester production and its potential use as bio lubricant, Ind. Crop. Prod. 43 (2013) 283–290, https://doi.org/10.1016/j.indcrop.2012.07.010.

[12] T.L. Greaves, C.J. Drummond, Protic ionic liquids: properties and applications, chem, Rev. 108 (2008) 206–237, https://doi.org/10.1021/cr068040u.

[13] M.D. Avilés, F.J. Carrión-Vilches, J. Sanes, M.D. Bermúdez, Diprotic ammonium succinate ionic liquid in thin film aqueous lubrication and in graphene nanolubricant, Tribol. Lett. 67 (2019) 26, https://doi.org/10.1007/s11249-019-1138-y.

[14] A. Arcifa, A. Rossi, S.N. Ramakrishna, R. Espinosa-Marzal, A. Sheehan, N. D. Spencer, Lubrication of Si-based tribopairs with a hydrophobic ionic liquid: the multiscale influence of water, J. Phys. Chem. C 122 (2018) 7331–7343, https://doi.org/10.1021/acs.jpcc.8b01671.

[15] Z. Tang, S. Li, A review of recent developments of friction modifiers for liquid lubricants (2007–present), Curr. Opin. Solid State Mater. Sci. 18 (2014) 119–139, https://doi.org/10.1016/j.cossms.2014.02.002.

[16] N. Saurín, M.D. Avilés, T. Espinosa, J. Sanes, F.J. Carrión, M.D. Bermúdez, P. Iglesias, Carbon nanophases in ordered nanofluid lubricants, Wear 376–377 (2017) 747–755, https://doi.org/10.1016/j.wear.2017.01.008.

[17] R. Pamies, M.D. Avilés, J. Arias-Pardilla, T. Espinosa, F.J. Carrión, J. Sanes, M. D. Bermúdez, Antiwear performance of ionic liquid+graphene dispersions with anomalous viscosity-temperature behavior, Tribol. Int. 122 (2018) 200–209, https://doi.org/10.1016/j.triboint.2018.02.020.

[18] L. Zhang, J. Pu, L. Wang, Q. Xue, Frictional dependence of graphene and carbon nanotube in diamond-like carbon/ionic liquids hybrid films in vacuum, Carbon 80 (2014) 734–745, https://doi.org/10.1016/j.carbon.2014.09.022.

[19] P. Rudenko, A. Bandyopadhyay, Talc as friction reducing additive to lubricating oil, Appl. Surf. Sci. 276 (2013) 383–389, https://doi.org/10.1016/j.apsusc.2013.03.102.

[20] M.R. Ortega Vega, J. Ercolani, S. Mattedi, C. Aguzzoli, C.A. Ferreira, A.S. Rocha, C. F. Malfatti, Oleate-based protic ionic liquids as lubricants for aluminum 1100, Ind. Eng. Chem. Res. 57 (2018) 12386–12396, https://doi.org/10.1021/acs.iecr.8b02426.

[21] T.E. Schmitzhaus, M.R. Ortega Vega, R. Schroeder, I.L. Muller, S. Mattedi, C. de F. Malfatti, An amino-based protic ionic liquid as a corrosion inhibitor of mild steel in aqueous chloride solutions, Materials and Corrosion, maco.201911347, https://doi.org/10.1002/maco.201911347, 2020.

[22] M.R. Ortega Vega, E.K. Baldin, D.P. Pereira, M.C.S. Martins, P. Pranke, F. Horn, I. Pinheiro, A. Vieira, B. Espiña, S. Mattedi, C. de F. Malfatti, Toxicity of oleate-based amino protic ionic liquids towards Escherichia coli, Danio rerio embryos and human skin cells, J. Hazard Mater. (2021), 126896, https://doi.org/10.1016/j.jhazmat.2021.126896.

[23] K. Nakayama, J.-M. Martin, Tribochemical reactions at and in the vicinity of a sliding contact, Wear 261 (2006) 235–240, https://doi.org/10.1016/j.wear.2005.10.012.

[24] P. Stemmer, A. Fischer, Pathways of dissipation of frictional energy under boundary lubricated sliding wear of martensitic materials, Lubricants 6 (2018) 34, https://doi.org/10.3390/lubricants6020034.

[25] M.D. Bermúdez, P. Iglesias, A.E. Jiménez, G. Martínez-Nicolás, Influence of sliding frequency on reciprocating wear of mold steel with different microstructures, Wear 267 (2009) 1784–1790, https://doi.org/10.1016/j.wear.2008.12.025.

[26] ASTM G133. Test Method for Linearly Reciprocating Ball-on-Flat Sliding Wear, ASTM International, 2016. https://doi.org/10.1520/G0133-05R16.

[27] L. Câmara Noronha, V. Velho de Castro, G.A. Ludwig, R. Moreira Schroeder, C. de Fraga Malfatti, Ti–Cp: eletrochemical behaviour under slurry erosion wear, J. Biol. Tribol. Corros. 7 (2020) 8, https://doi.org/10.1007/s40735-020-00442-y.

[28] R.L. Dalcin, L.F. Oliveira, I.L. Diehl, V.W. Dias, A. da S. Rocha, Response of a DIN 18MnCrSiMo6-4 continuous cooling bainitic steel to plasma nitriding with a nitrogen rich gas composition, Mater. Res. 23 (2020), e20200036, https://doi.org/10.1590/1980-5373-mr-2020-0036.

[29] R.L. Dalcin, A. da S. Rocha, V.V. de Castro, J.C.K. das Neves, C.H. da Silva, R. D. Torres, R.M. Nunes, C. de F. Malfatti, Microstructure and wear properties of a low carbon bainitic steel on plasma nitriding at different N₂-H₂ gas mixtures, Mater. Res. 25 (2021), https://doi.org/10.1590/1980-5373-MR-2021-0447.

[30] R.C. Morón, I. Hernández-Onofre, A.D. Contla-Pacheco, D. Bravo-Bárcenas, I. Campos-Silva, Friction and reciprocating wear behavior of borided AISI H13 steel under dry and lubricated conditions, J. Mater. Eng. Perform. (2020), https://doi.org/10.1007/s11665-020-04957-w.

[31] D.L. Burris, W.G. Sawyer, Measurement uncertainties in wear rates, Tribol. Lett. 36 (2009) 81–87, https://doi.org/10.1007/s11249-009-9477-8.

[32] ASTM G102 - 89(2015)e1 Standard Practice for Calculation of Corrosion Rates and Related Information from Electrochemical Measurements, n.d. https://www.astm.org/Standards/G102. (Accessed 8 November 2021). accessed.

[33] F.J. Profito, Modelagem unidimensional do regime misto de lubrificação aplicada a superfícies texturizadas, Mestrado em Engenharia de Controle e Automação Mecânica, Universidade de São Paulo, 2011, https://doi.org/10.11606/D.3.2011.tde-29112010-155407.

[34] H.A. Spikes, Film-forming additives - direct and indirect ways to reduce friction, Lubric. Sci. 14 (2002) 147–167, https://doi.org/10.1002/ls.3010140204.

[35] A.K. Jha, T.K. Dan, S.V. Prasad, P.K. Rohatgi, Aluminium alloy-solid lubricant talc particle composites, J. Mater. Sci. 21 (1986) 3681–3685, https://doi.org/10.1007/BF00553819.

[36] B. Rotenberg, A.J. Patel, D. Chandler, Molecular explanation for why talc surfaces can Be both hydrophilic and hydrophobic, J. Am. Chem. Soc. 133 (2011) 20521–20527, https://doi.org/10.1021/ja208687a.

[37] G.E. Morris, D. Fornasiero, J. Ralston, Polymer depressants at the talc–water interface: adsorption isotherm, microflotation and electrokinetic studies, Int. J. Miner. Process. 67 (2002) 211–227, https://doi.org/10.1016/S0301-7516(02)00048-0.

[38] S.H. Kumar, S.K. J, S.A. K, Estimatation of talc properties after milling, AIP Conf. Proc. 1728 (2016), 020139, https://doi.org/10.1063/1.4946190.

[39] J. Ann Bazar, M. Rahimi, S. Fathinia, M. Jafari, V. Chipakwe, S. Chehreh Chelgani, Talc flotation—an overview, Minerals 11 (2021) 662, https://doi.org/10.3390/min11070662.

[40] L.H. Allen, W.A. Cavanagh, J.E. Holton, G.R. Williams, New understanding of talc addition may help improve control of pitch, Pulp and Paper (USA). https://scholar.google.com/scholar_lookup?title=New+understanding+of+talc+addition+may+help+improve+control+of+pitch&author=Allen%2C+L.H.&publication_year=1993, 1993. (Accessed 20 October 2021). accessed.

[41] P. Schatzberg, Investigation of Sorbents for Removing Oil Spills from Waters, NAVAL SHIP RESEARCH AND DEVELOPMENT LAB ANNAPOLIS MD, 1971. https://apps.dtic.mil/sti/citations/AD0742950. (Accessed 20 October 2021). accessed.

[42] D. Zadaka-Amir, N. Bleiman, Y.G. Mishael, Sepiolite as an effective natural porous adsorbent for surface oil-spill, Microporous Mesoporous Mater. 169 (2013) 153–159, https://doi.org/10.1016/j.micromeso.2012.11.002.

[43] V.H. Álvarez, S. Mattedi, M. Martin-Pastor, M. Aznar, M. Iglesias, Synthesis and thermophysical properties of two new protic long-chain ionic liquids with the oleate anion, Fluid Phase Equil. 299 (2010) 42–50, https://doi.org/10.1016/j.fluid.2010.08.022.

[44] Stribeck Curves In Reciprocating Test (n.d.), https://www.bruker.com/en/products-and-solutions/test-and-measurement/tribometers-and-mechanical-testers/stribeck-curves-in-reciprocating-test.html. accessed May 20, 2022.

[45] H. Guo, T. Smith, P. Iglesias, The study of hexanoate-based protic ionic liquids used as lubricants in steel-steel contact, J. Mol. Liq. (2019), 112208, https://doi.org/10.1016/j.molliq.2019.112208.

[46] J. Qu, P.J. Blau, S. Dai, H. Luo, H.M. Meyer, Ionic liquids as novel lubricants and additives for diesel engine applications, Tribol. Lett. 35 (2009) 181–189, https://doi.org/10.1007/s11249-009-9447-1.

[47] S.M. Hsu, R.S. Gates, Boundary lubricating films: formation and lubrication mechanism, Tribol. Int. 38 (2005) 305–312, https://doi.org/10.1016/j.triboint.2004.08.021.

[48] T.F.J. Quinn, J.L. Sullivan, D.M. Rowson, Origins and development of oxidational wear at low ambient temperatures, Wear 94 (1984) 175–191, https://doi.org/10.1016/0043-1648(84)90053-X.

[49] S. Bair, F. Qureshi, W.O. Winer, Observations of shear localization in liquid lubricants under pressure, J. Tribol. 115 (1993) 507–513, https://doi.org/10.1115/1.2921667.

[50] A. Raj, K. Raju, H.T. Varghese, C.M. Granadeiro, H.I.S. Nogueira, C.Y. Panicker, IR, Raman and SERS spectra of 2-(methoxycarbonylmethylsulfanyl)-3,5-dinitrobenzene carboxylic acid, J. Braz. Chem. Soc. 20 (2009) 549–559, https://doi.org/10.1590/S0103-50532009000300021.

[51] Complementarity of Raman and Infrared Spectroscopy for Structural Characterization of Plant Epicuticular Waxes | ACS Omega (n.d.), https://pubs.acs.org/doi/10.1021/acsomega.8b03675. (Accessed 4 January 2022). accessed.

[52] Infrared and Raman Spectroscopy - 1st Edition (n.d.), https://www.elsevier.com/books/infrared-and-raman-spectroscopy/larkin/978-0-12-386984-5. (Accessed 4 January 2022). accessed.

[53] W.G. Cui, Q.B. Lai, L. Zhang, F.M. Wang, Quantitative measurements of sp3 content in DLC films with Raman spectroscopy, Surf. Coating. Technol. 205 (2010) 1995–1999, https://doi.org/10.1016/j.surfcoat.2010.08.093.

[54] H. Pang, X. Wang, G. Zhang, H. Chen, G. Lv, S. Yang, Characterization of diamond-like carbon films by SEM, XRD and Raman spectroscopy, Appl. Surf. Sci. 256 (2010) 6403–6407, https://doi.org/10.1016/j.apsusc.2010.04.025.

[55] M.C. Tosin, A.C. Peterlevitz, G.I. Surdutovich, V. Baranauskas, Deposition of diamond and diamond-like carbon nuclei by electrolysis of alcohol solutions, Appl. Surf. Sci. (1999) 260–264.

[56] C. Qi, D. Zhang, S. Gao, H. Ma, Y. He, S. Ma, Y. Chen, X. Yang, Crystal structure and magnetic property of a metal-organic framework (MOF) containing double-stranded chain with metallomacrocycles and dinuclear Mn(II) subunits, J. Mol. Struct. 1–3 (2008) 357–363, https://doi.org/10.1016/j.molstruc.2008.04.008.

[57] H. Xiao, D. Guo, S. Liu, G. Pan, X. Lu, Film thickness of ionic liquids under high contact pressures as a function of alkyl chain length, Tribol. Lett. 41 (2011) 471–477, https://doi.org/10.1007/s11249-010-9729-7.

[58] J. Wu, Y. Luo, Y. Chen, X. Lu, X. Feng, N. Bao, Y. Shi, Poly(ionic liquid)s as lubricant additives with insight into adsorption-lubrication relationship, Tribol. Int. 165 (2022), 107278, https://doi.org/10.1016/j.triboint.2021.107278.

[59] H. Kondo, Protic ionic liquids with ammonium salts as lubricants for magnetic thin film media, Tribol. Lett. 31 (2008) 211–218, https://doi.org/10.1007/s11249-008-9355-9.

[60] G. Huang, Q. Yu, Z. Ma, M. Cai, W. liu, Probing the lubricating mechanism of oil-soluble ionic liquids additives, Tribol. Int. 107 (2017) 152–162, https://doi.org/10.1016/j.triboint.2016.08.027.

[61] Tribological performance of phosphonium based ionic liquids for an aluminum-on-steel system and opinions on lubrication mechanism - ScienceDirect, n.d. https://www.sciencedirect.com/science/article/pii/S0043164806001384. (Accessed 5 November 2021). accessed

[62] S.M. Hsu, J. Zhang, Z. Yin, The nature and origin of tribochemistry, Tribol. Lett. 13 (2002) 131–139, https://doi.org/10.1023/A:1020112901674.

[63] Y.Z. Zhan, G. Zhang, Mechanical mixing and wear-debris formation in the dry sliding wear of copper matrix composite, Tribol. Lett. 17 (2004) 581–592, https://doi.org/10.1023/B:TRIL.0000044508.54186.66.

[64] D.A. Rigney, L.H. Chen, M.G.S. Naylor, A.R. Rosenfield, Wear processes in sliding systems, Wear 100 (1984) 195–219, https://doi.org/10.1016/0043-1648(84)90013-9.

[65] A.S. Reddy, B.N.P. Bai, K.S.S. Murthy, S.K. Biswas, Wear and seizure of binary Al—Si alloys, Wear 171 (1994) 115–127, https://doi.org/10.1016/0043-1648(94)90354-9.

[66] D.L.A. de Faria, S. Venâncio Silva, M.T. de Oliveira, Raman microspectroscopy of some iron oxides and oxyhydroxides, J. Raman Spectrosc. 28 (1997) 873–878, https://doi.org/10.1002/(SICI)1097-4555(199711)28:11<873::AID-JRS177>3.0.CO;2-B.

[67] T.F.J. Quinn, NASA Interdisciplinary Collaboration in Tribology, (n.d.) 118.

[68] A.W. Batchelor, G.W. Stachowiak, A. Cameron, The relationship between oxide films and the wear of steels, Wear 113 (1986) 203–223, https://doi.org/10.1016/0043-1648(86)90121-3.

[69] R.M. Crockett, M.P. Derendinger, P.L. Hug, S. Roos, Wear and electrical resistance on diesel lubricated surfaces undergoing reciprocating sliding, Tribol. Lett. 16 (2004) 187–194, https://doi.org/10.1023/B:TRIL.0000009729.15103.5c.

[70] Microstructure and Wear of Materials - 1st Edition, n.d. https://www.elsevier.com/books/microstructure-and-wear-of-materials/zum-gahr/978-0-444-42754-0. (Accessed 4 April 2022). accessed

[71] L.J. Basile, J.R. Ferraro, M.L. Mitchell, J.C. Sullivan, The Raman scattering of actinide (VI) ions in carbonate media, Appl. Spectrosc. 32 (1978) 535–537.

[72] A. Mäntyranta, V. Heino, E. Isotahdon, T. Salminen, E. Huttunen-Saarivirta, Tribocorrosion behaviour of two low-alloy steel grades in simulated waste solution, Tribol. Int. 138 (2019) 250–262, https://doi.org/10.1016/j.triboint.2019.05.032.

[73] V.V. de Castro, L.A. Mazzini Fontoura, J.D. Benfica, M. Seferin, J.L. Pacheco, C. A. dos Santos, Lubricated sliding wear of SAE 1045 and SAE 52100 steel against alumina in the presence of biodiesel, diesel and a 50:50 blend of those fuels, Wear 368–369 (2016) 267–277, https://doi.org/10.1016/j.wear.2016.09.026.

[74] S. Xing, S. Yu, Y. Deng, M. Dai, L. Yu, Effect of cerium on abrasive wear behaviour of hardfacing alloy, J. Rare Earths 30 (2012) 69–73, https://doi.org/10.1016/S1002-0721(10)60641-2.

[75] P.K. Katiyar, S. Misra, K. Mondal, Comparative corrosion behavior of five microstructures (pearlite, bainite, spheroidized, martensite, and tempered martensite) made from a high carbon steel, Metall. Mater. Trans. 50 (2019) 1489–1501, https://doi.org/10.1007/s11661-018-5086-1.

[76] D. Clover, B. Kinsella, B. Pejcic, R. De Marco, The influence of microstructure on the corrosion rate of various carbon steels, J. Appl. Electrochem. 35 (2005) 139–149, https://doi.org/10.1007/s10800-004-6207-7.

[77] Michel Dubus, et al., Atmospheric Corrosion Monitoring on Silver in Museums, n.d. http://www.iaq.dk/iap/iaq2003/2003_15.htm. (Accessed 12 November 2021). accessed